Nanowires for Thermoelectric Applications

M. S. Dresselhaus

Massachusetts Institute of Technology

Group members

Yu-Ming Lin
Steve B. Cronin
Marcie R. Black
Oded Rabin
Dr. Gene Dresselhaus

Collaborators

Prof. Gang Chen
Dr. Jos Heremans
Prof. Jackie Y. Ying

Introduction to Low Dimensions

- Density of states and predicted *ZT*:

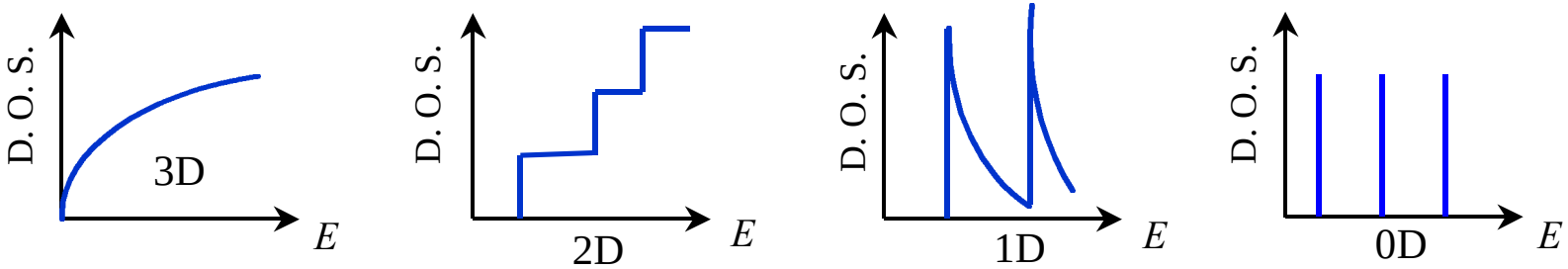

- Promising low-dimensional systems:
  - 2D Quantum Wells: $PbTe/PbEu_{1-x}Te_x$
    Si/Ge and GaAs/AlAs
  - 1D Quantum Wires: Bi and $Bi_{1-x}Sb_x$
  - 0D Quantum Dots: $PbSe_xTe_{1-x}$
    segmented nanowires

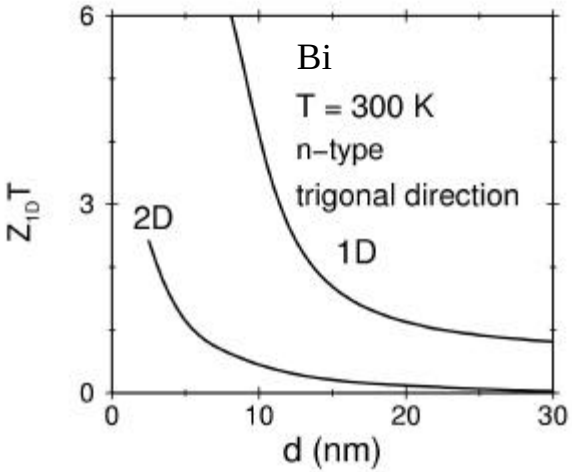

Inter-Group Activities

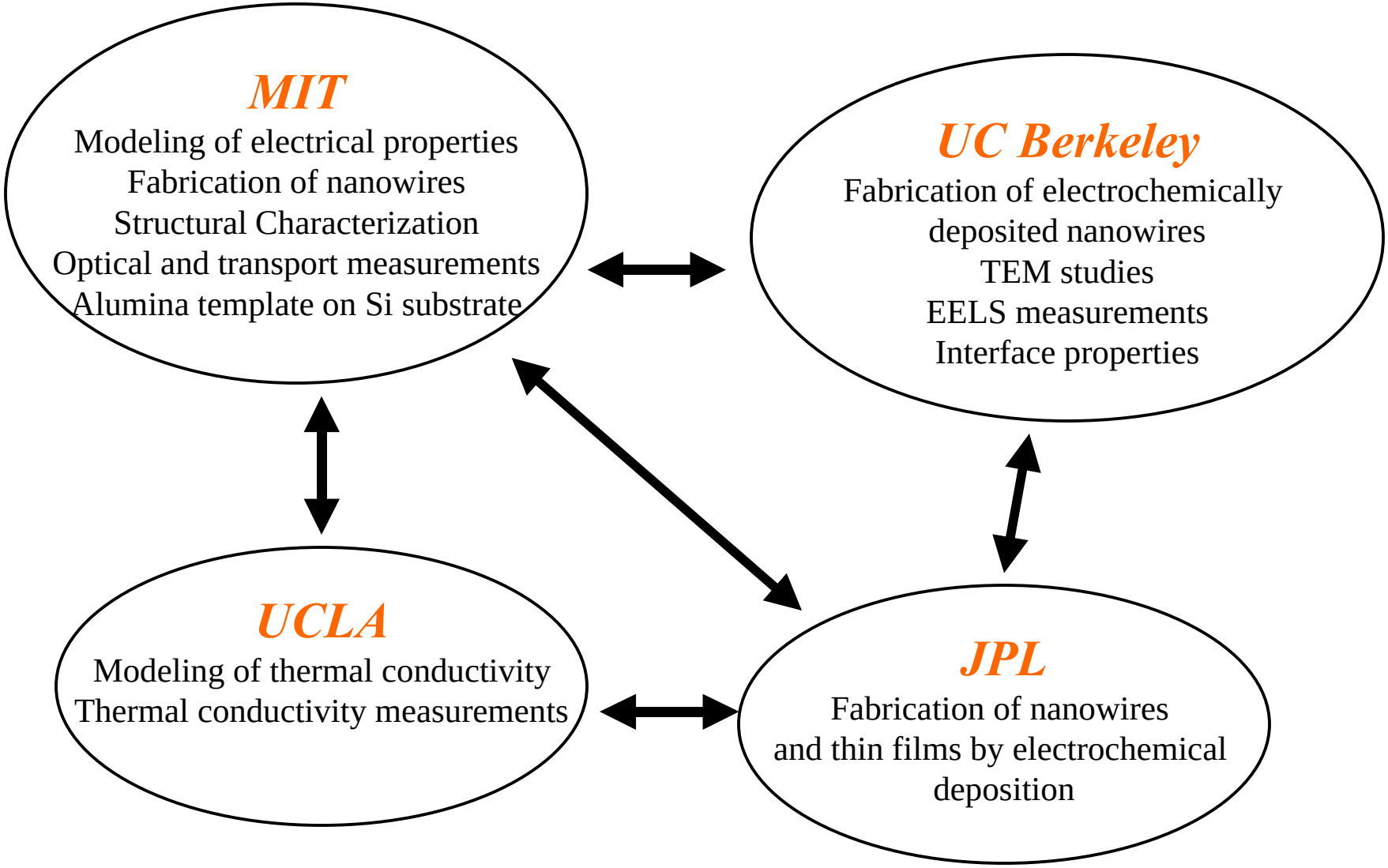

Template-Assisted Nanowire Fabrication

- Synthesis of porous templates (e.g., anodic alumina)
- Filling of nanopores with target material
  - Pressure injection
  - Vapor deposition
  - Electrochemical deposition
- Post-filling treatment

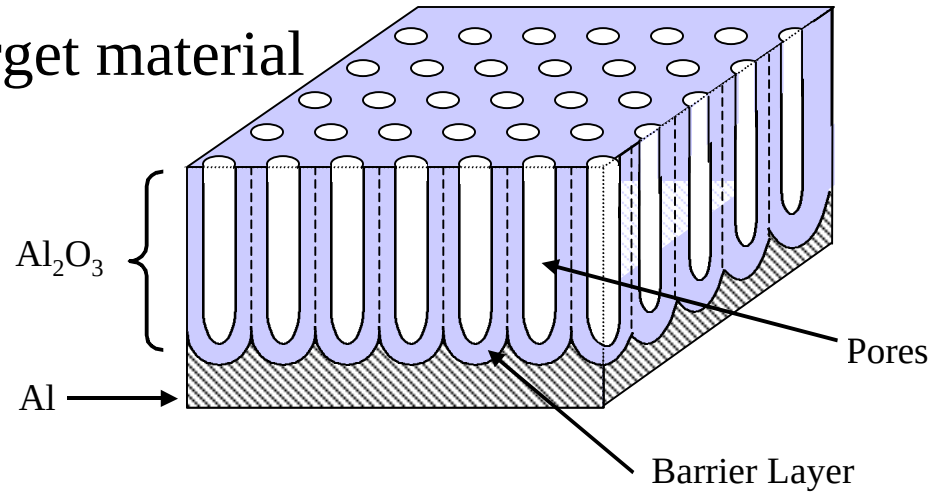

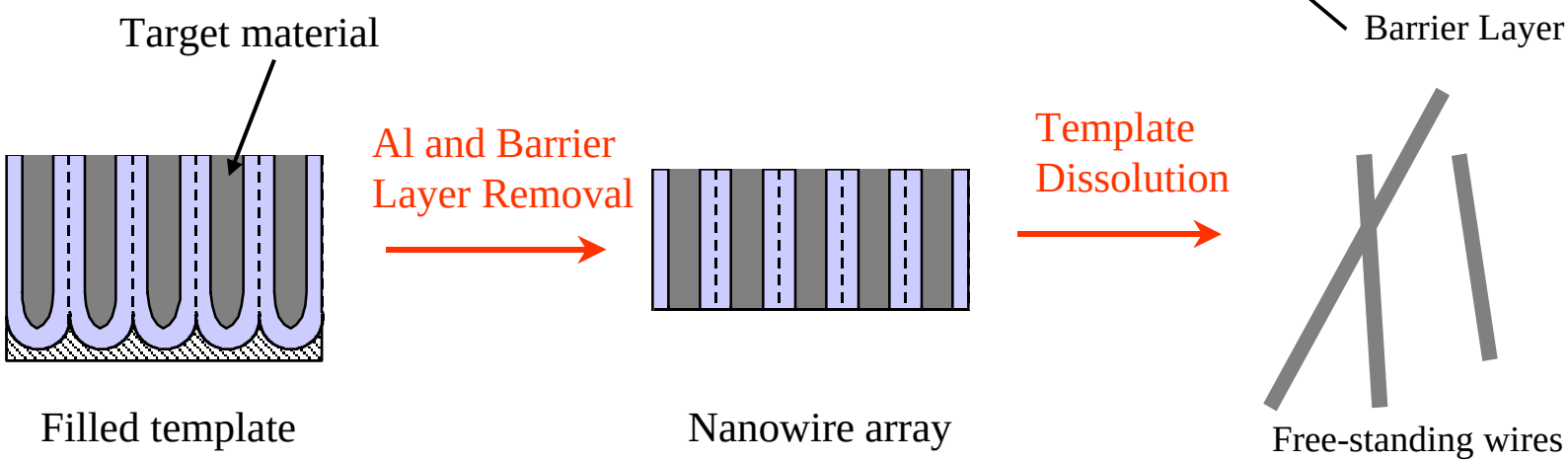

Synthesis of Nanowires

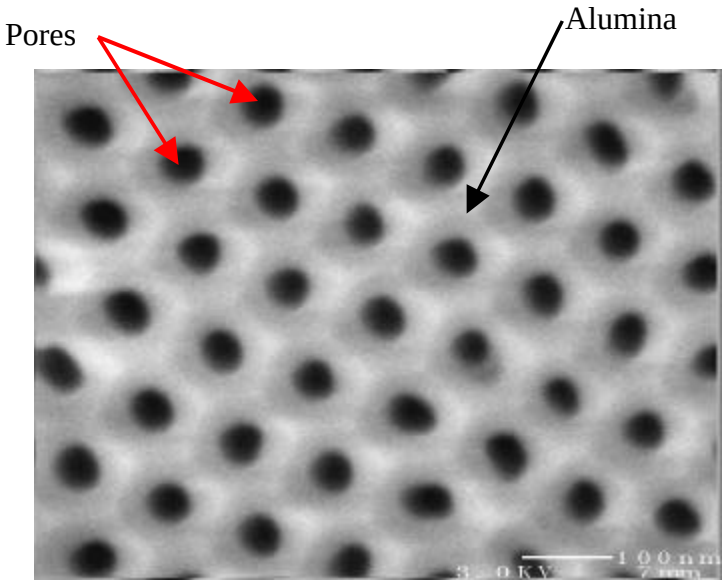

SEM image of top surface of porous alumina anodized in 4 wt% $H_2C_2O_4$ at 45 V. The pore diameter is ~ **44** nm.

Pressure Injection

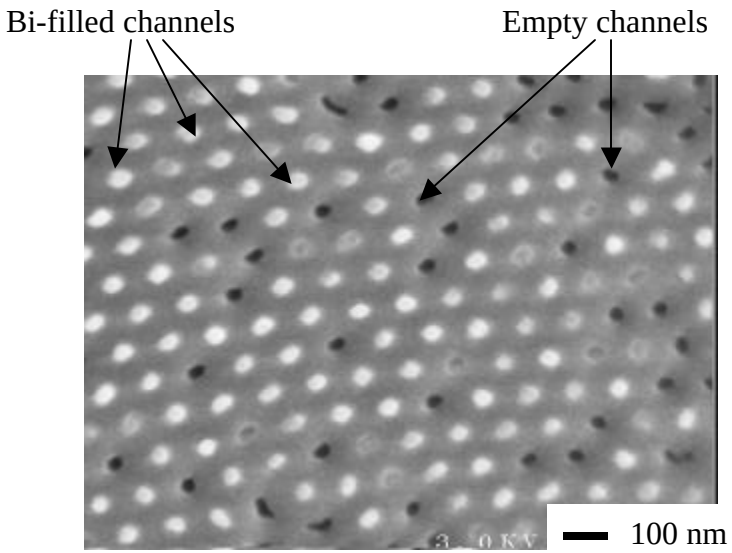

SEM image of bottom surface of Bi nanowire arrays after the barrier layer has been removed. The wire diameter is ~ **40** nm.

Theoretical Modeling for Cylindrical Wires

Schrödinger equation for anisotropic carriers

$$-\hbar^2 \nabla \cdot \frac{1}{2\vec{m}} \cdot \nabla y + U(\vec{r})y = Ey$$

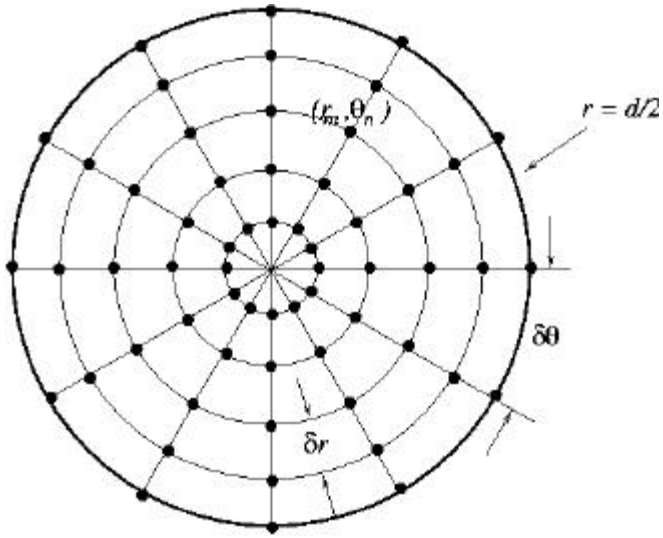

Grid points for calculating wavefunctions in cylindrical Bi nanowires.

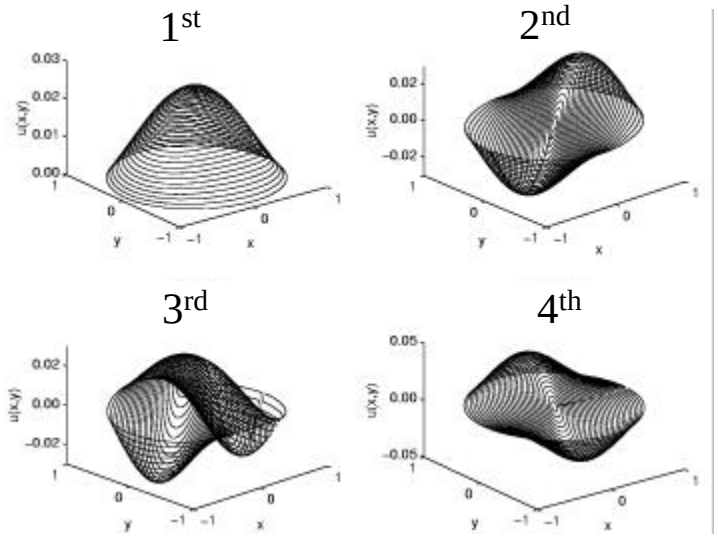

Calculated wavefunction in cylindrical Bi nanowires (for the lowest four states).

Semimetal-Semiconductor Transition in Bi

- Bi
  - Group V element
  - Semimetal in bulk form
  - The conduction band (*L*-electron) overlaps with the valence band (*T*-hole) by 38 meV
- Bi nanowire
  - Semimetal-semiconductor transition at a wire diameter about 50 nm due to quantum confinement effects

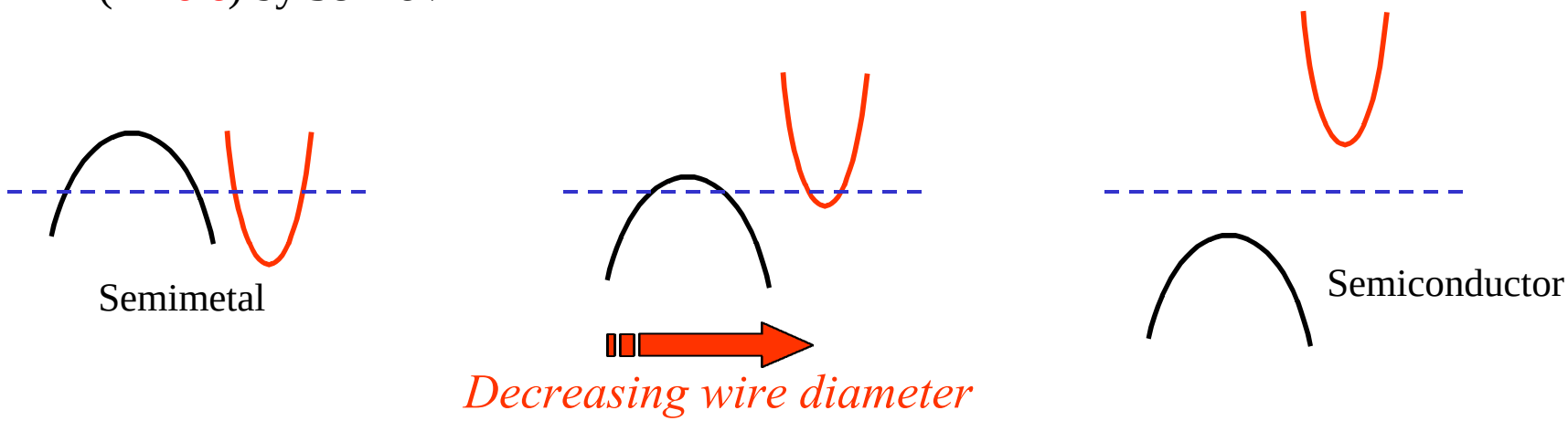

Critical wire diameters (in nm)

Direction	Trigonal	Binary	Bisectrix	(101)	(012)
R (nm)	55.1	39.8	48.5	48.7	49.0

Measured $R(T)$ of Bi Nanowire Arrays

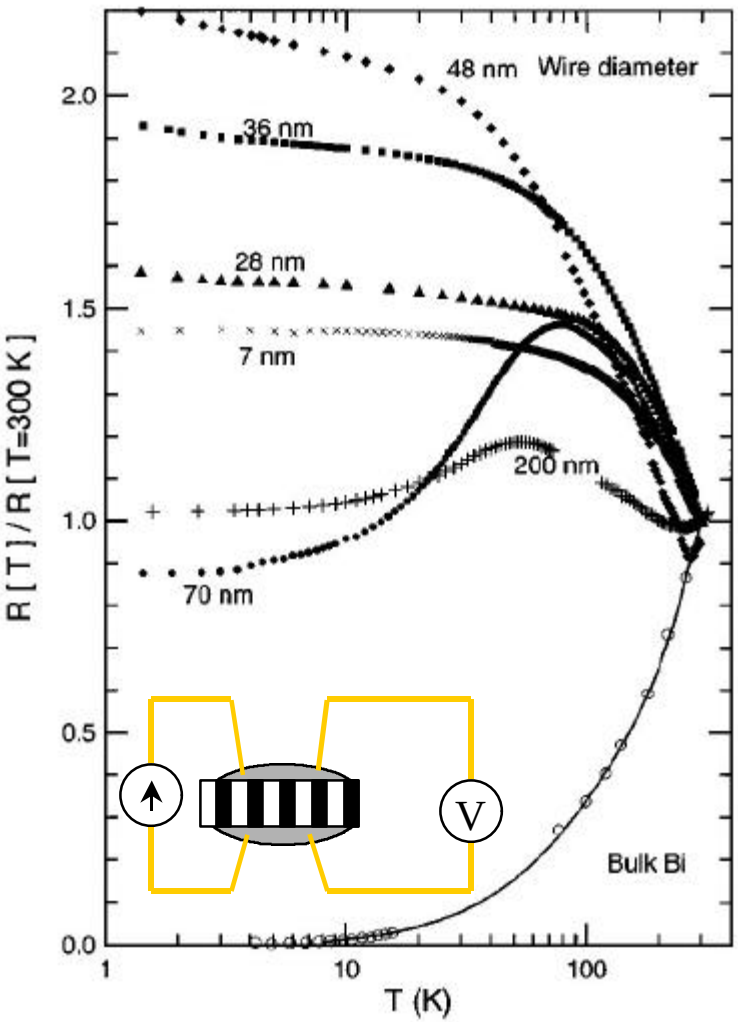

Theoretical Modeling:

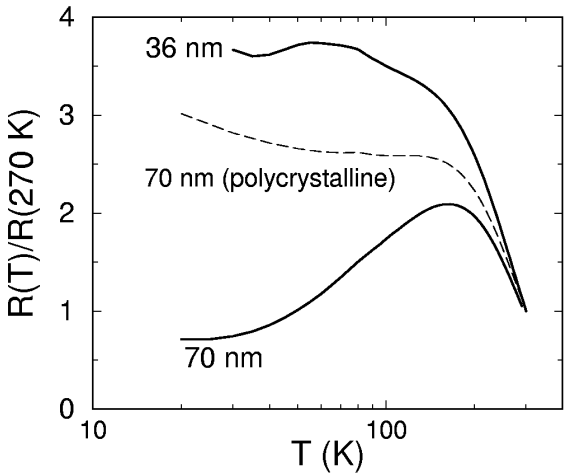

- Matthiessen's rule:

$$\frac{1}{\mu_{tot}} = \frac{1}{\mu_{bulk}} + \frac{1}{\mu_{boundary}} + \frac{1}{\mu_{imp}}$$

Measured $R(T)$ for different wire diameters. [J. Heremans *et al.*]

- Established the validity of the theoretical modeling
- Evidence for the semimetal - semiconductor transition

$R(T)$ of Te-doped Bi Nanowires

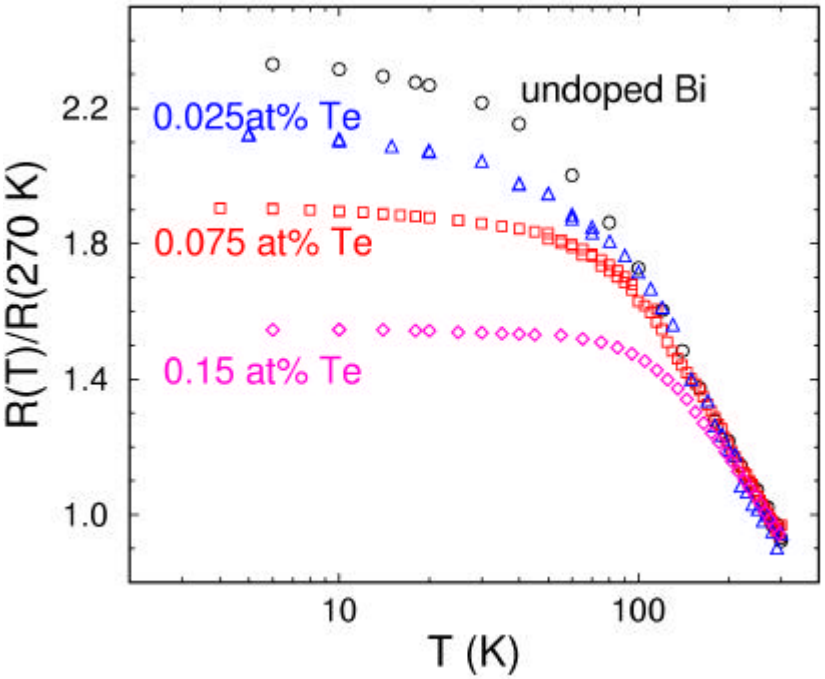

Experimental $R(T)$ of 40-nm Te-doped Bi nanowires

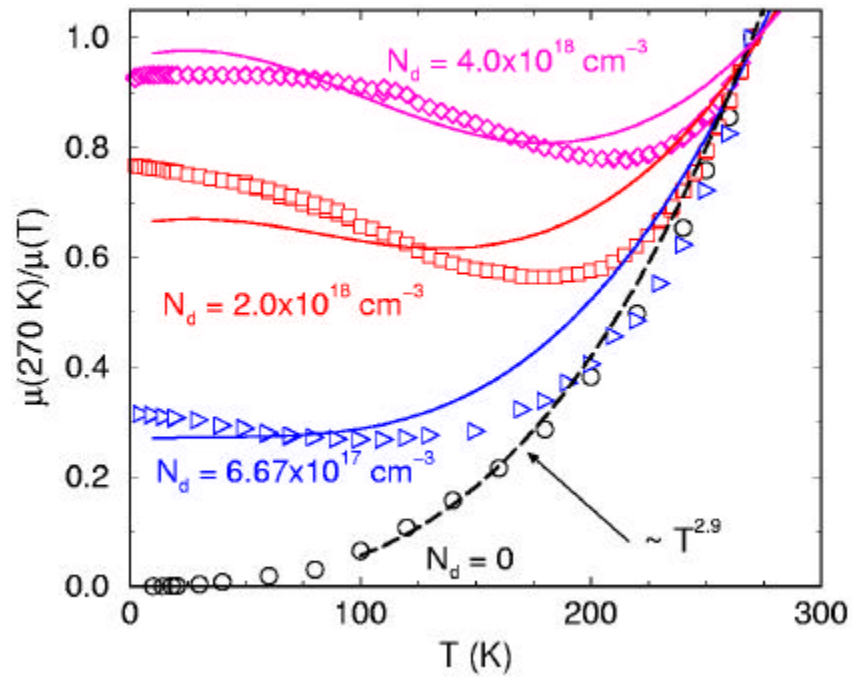

Effective mobility $\mu(T)$
Compared with theory

- **The transport model is able to explain and predict *T*-dependent resistance of Bi and Te-doped Bi nanowires**

Polarization Effects

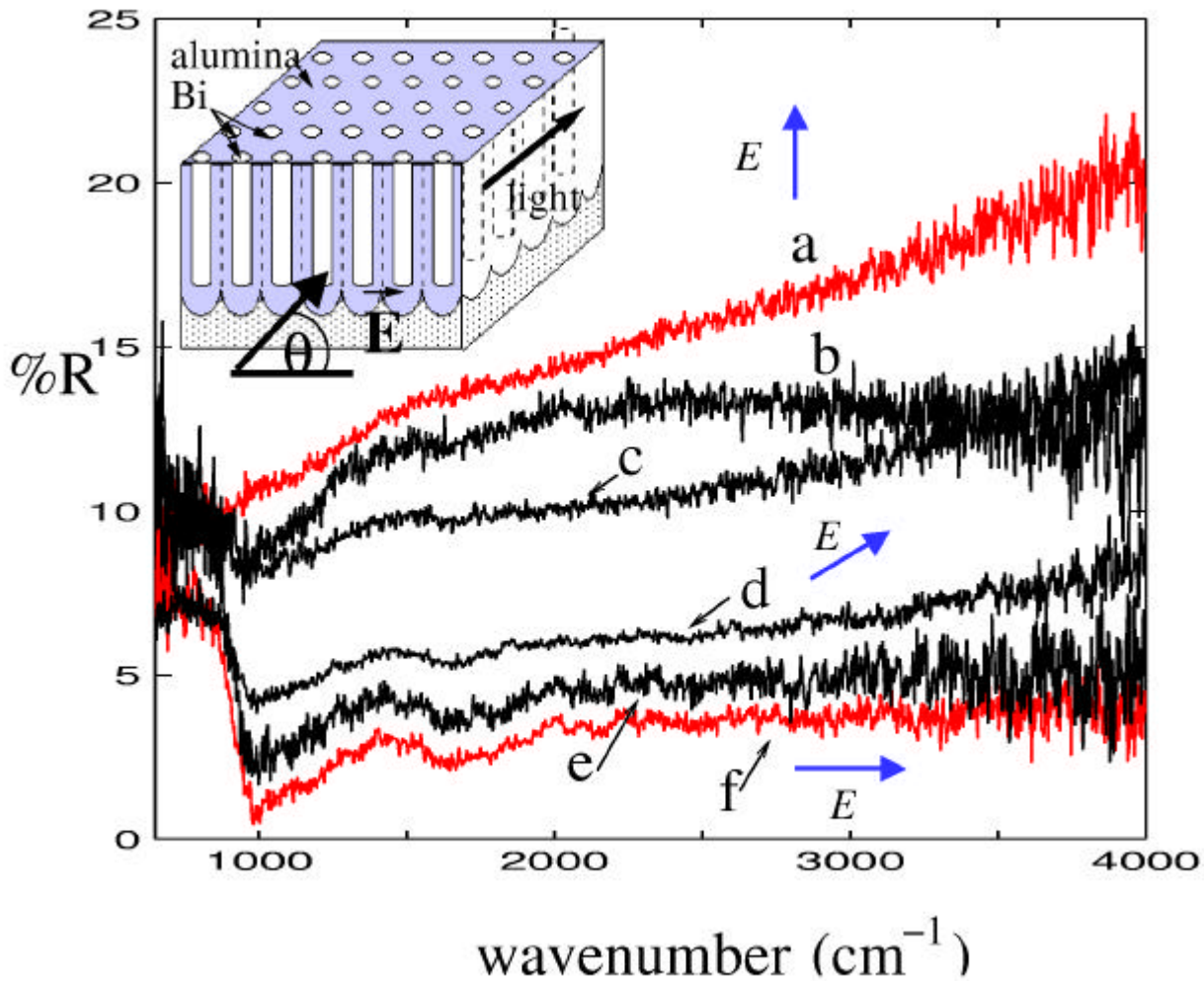

Reflectivity of a Bi/Alumina composite with different polarization angles: (a) 90º, (b) 117º, (c) 63º, (d) 27º, (e) -27º, and (f) 0º. The results are consistent with the selection rules for an inter-subband transition.

Measurements of Individual Bi Nanowires

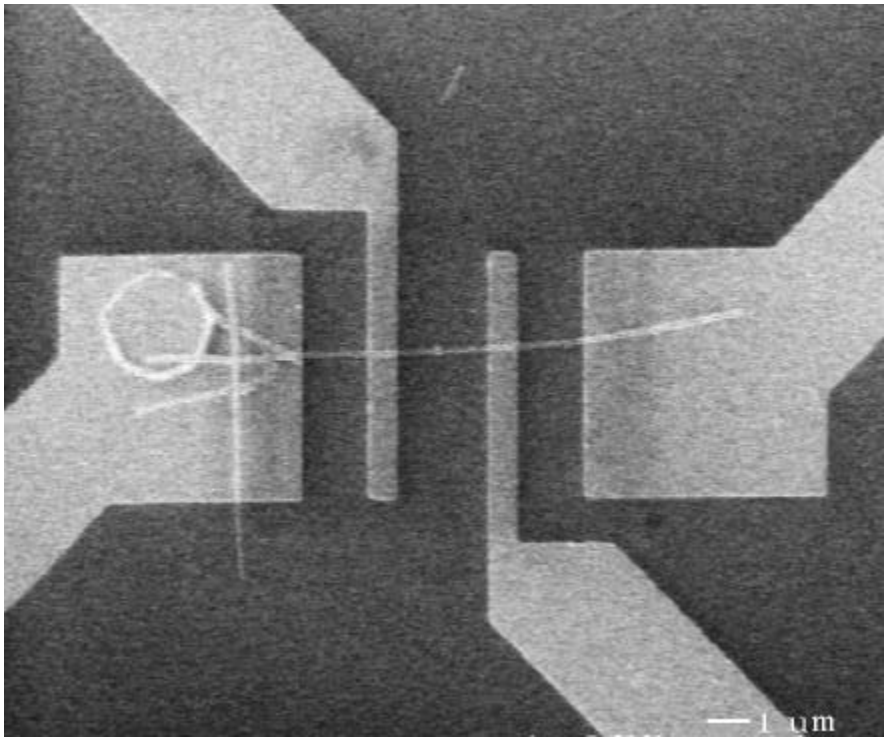

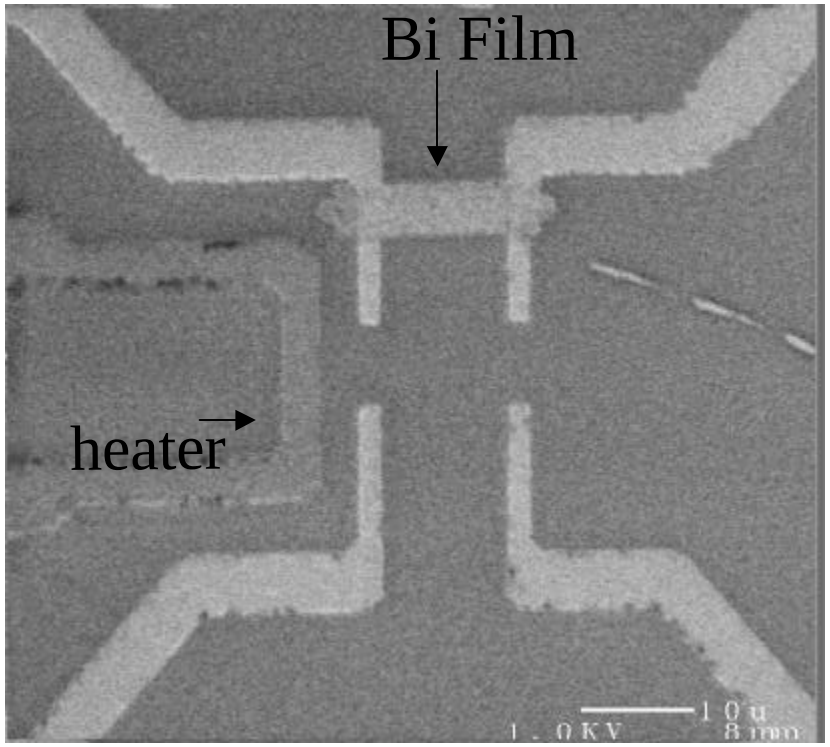

4-Point Resistivity Measurement

- Contact resistance > 1MΩ
- Non-linear I-V

Differential Seebeck Measurement

- Seebeck measured with respect to known bulk Bi film

$$S = \frac{\Delta V}{\Delta T}$$

- ΔT~ 0.5 K easily attained

4-Point Measurement at Room Temperature of a 200 nm Bi nanowire after FIB treatment

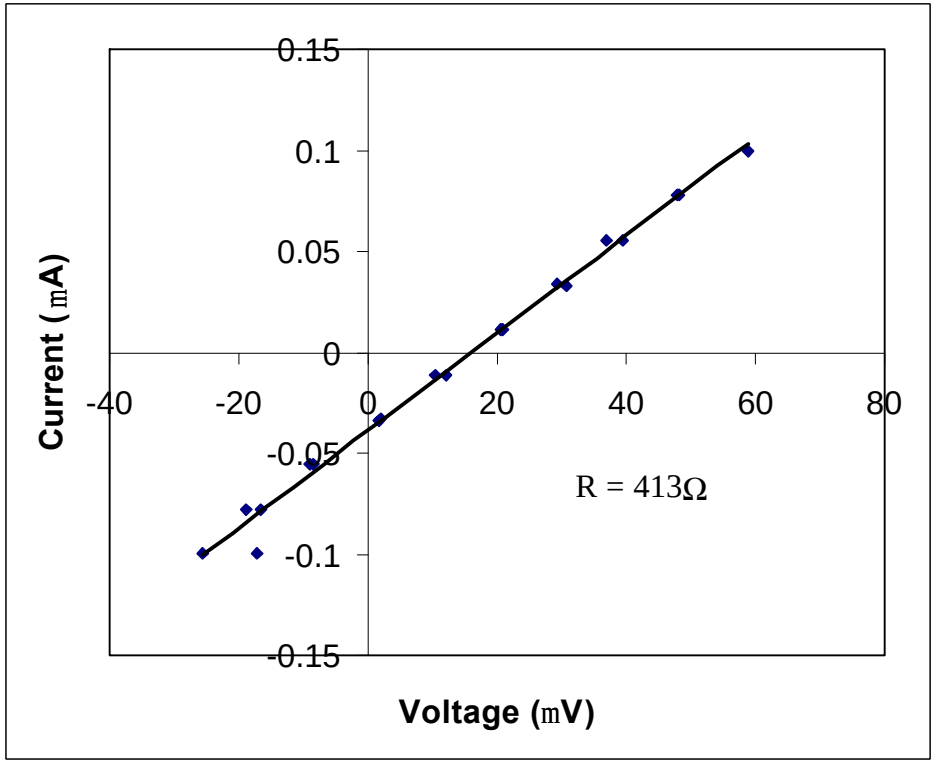

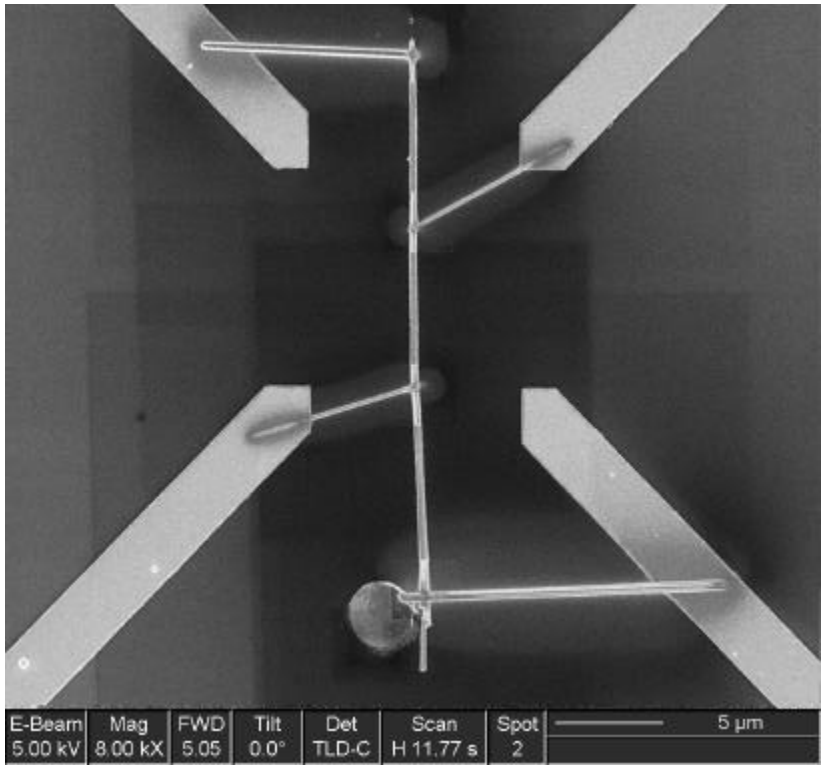

Diameter = 200nm
Length = 6.9µm
R_{sample} = 413Ω
$R_{contacts}$ = 4kΩ
T=300K

$$r_{sample} = \frac{R \cdot A}{L} = 1.88 \times 10^{-4} \Omega \cdot cm$$

$$r_{bulk} = 1.2 \times 10^{-4} \Omega \cdot cm$$

Major Progress for Four Years

- Improved the theoretical model of nanowire systems by explicitly considering the cylindrical geometry, the crystalline anisotropy, and the temperature dependence of the materials properties. This allowed detailed calculation of semimetal-semiconductor transition in Bi nanowires
- Confirmed the model with experimental results in temperature-dependent resistance measurements for various diameters and Te concentrations.
- Fabricated undoped Bi, Te-doped Bi, and $Bi_{1-x}Sb_x$ nanowire arrays with uniform diameters in the range 7-110 nm, and found a wire diameter-dependent crystal orientation along the wire axis. The nanowires are of high crystalline quality, as characterized by XRD and HRTEM.
- Made progress on single wire measurements by exploiting various techniques (EB lithography + FIB milling/deposition).
- Fabricated ordered porous alumina templates on a large (10 cm in size) Si substrate, and evaluated the possibility to incorporate nanowires with electronic, optical devices on the wafer.
- Measured optical properties of nanowire arrays, and optical absorption results have been related to model calculations.

Alumina Templates on Silicon Wafers

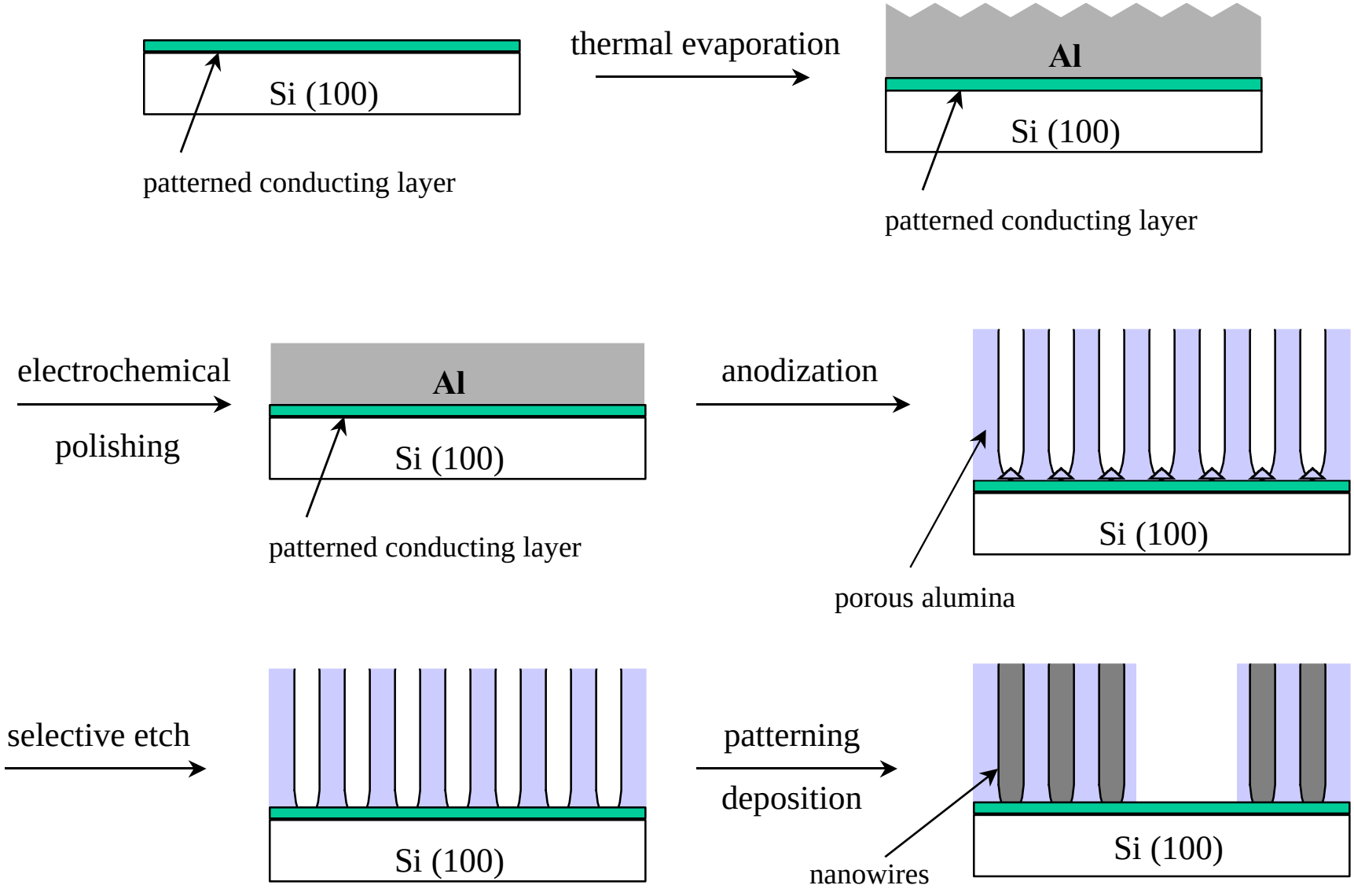

Towards Multi-Component Nanowire Arrays

By means of lithography, a design allowing deposition of both *p*-type and *n*-type components on the same support could be achieved.

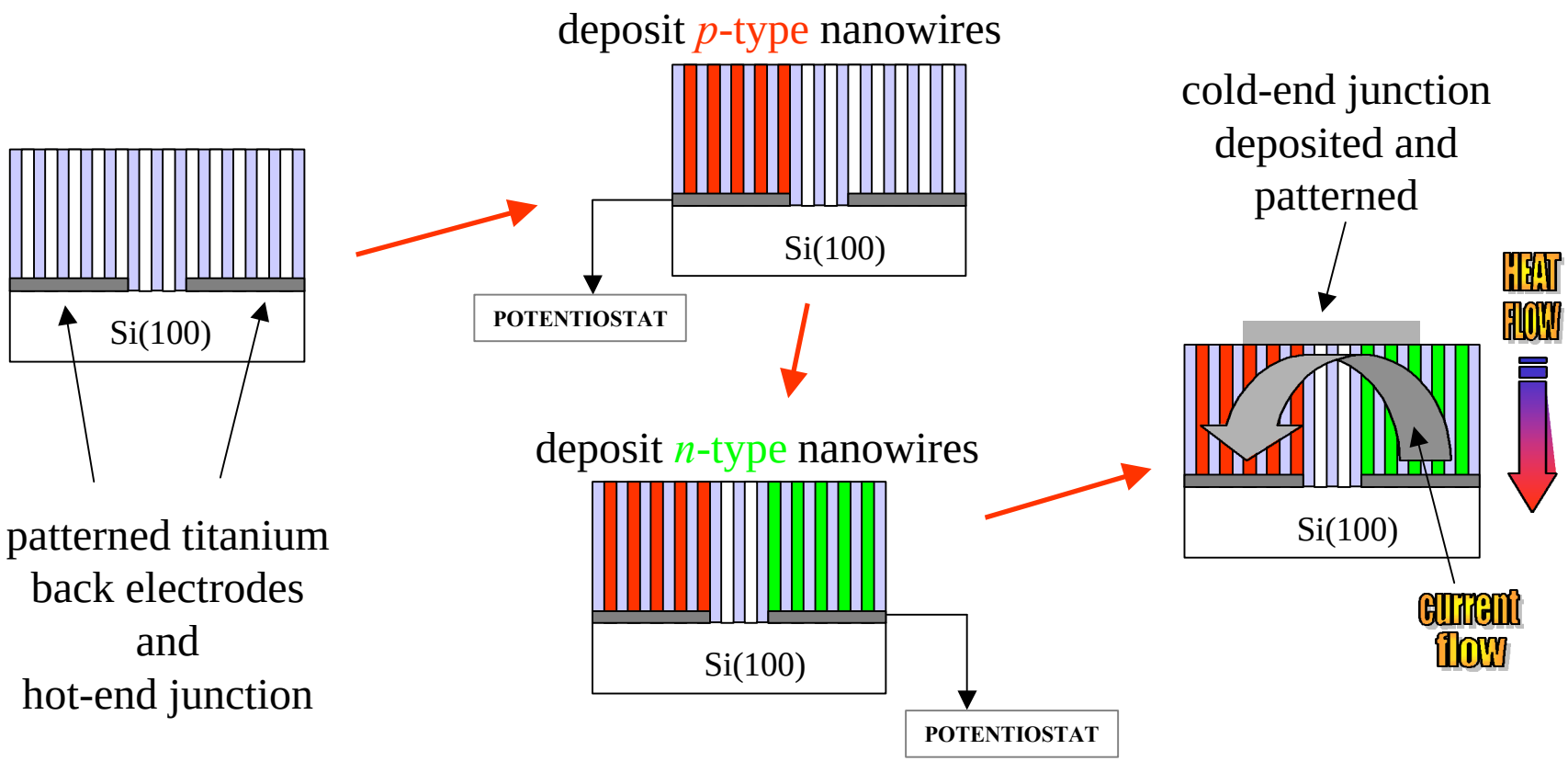

Electrochemical Deposition of Bismuth Nanowires

Bismuth deposition is commonly carried out from electrolytes with extreme pH values due to solubility problems. The porous alumina template, however, is prone to dissolution at pH<5 and pH>9.

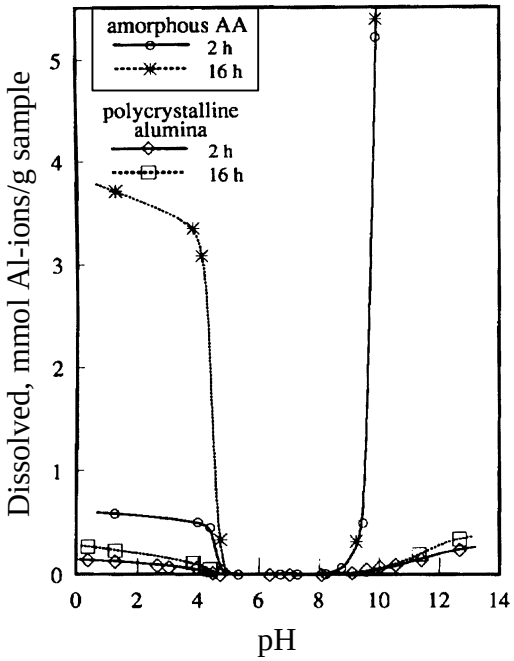

Paterson *et.al., J. Membrane Sci.* **98**,143(1995)

Arrays of bismuth nanowires were prepared in porous alumina templates (PAA) by deposition from a nearly **neutral** electrolyte (pH~6), using EthyleneDiamineTetraAcetic acid (EDTA) to prevent precipitation of Bi salts.

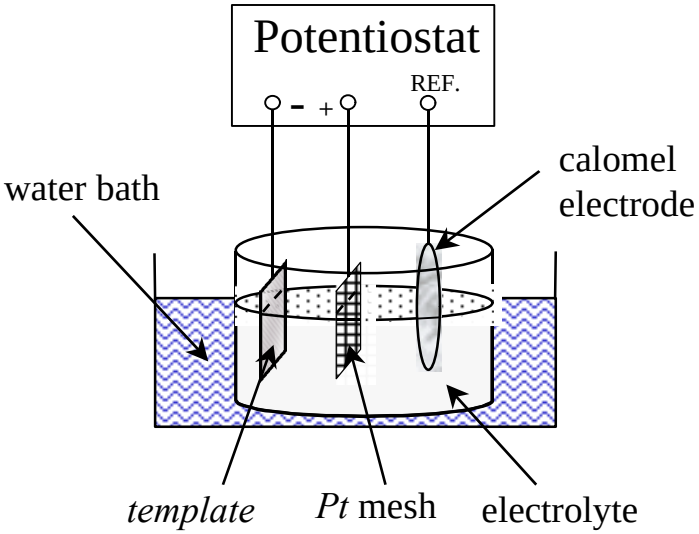

- Electrolyte composition:
  - 40mM Bismuth Nitrate Hydrate
  - 70mM EDTA
- Deposition at a constant voltage of -670*mV* vs. saturated calomel electrode.

Nanowire Deposition in Alumina

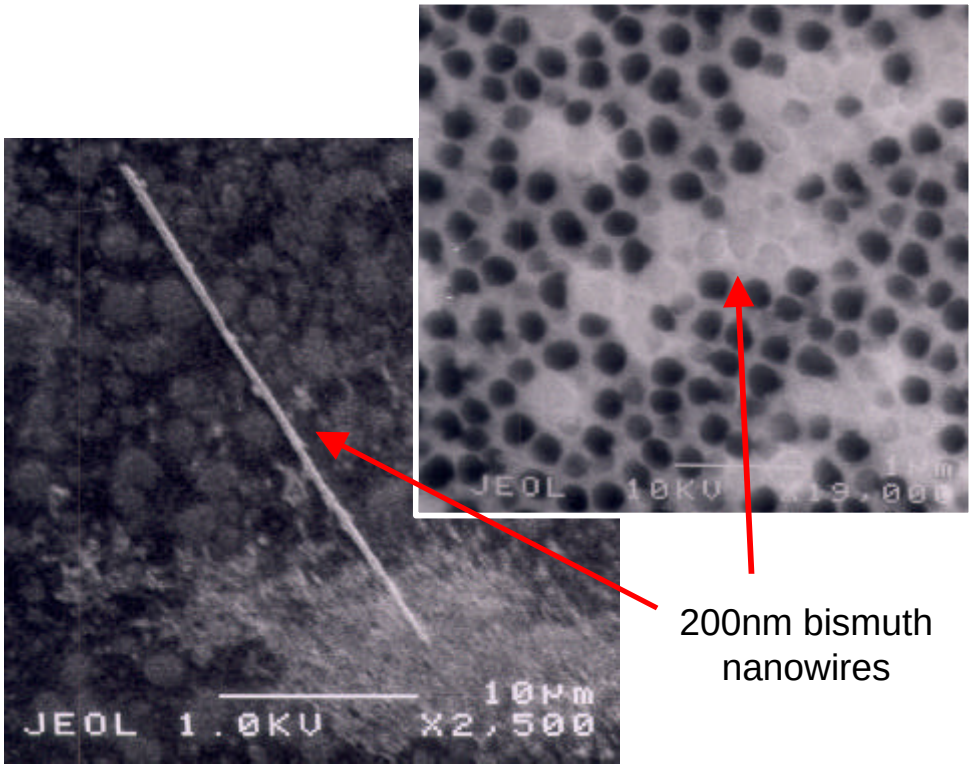

200-nm Bi nanowires deposited in a commercial PAA with a vacuum deposited Au film back-electrode.

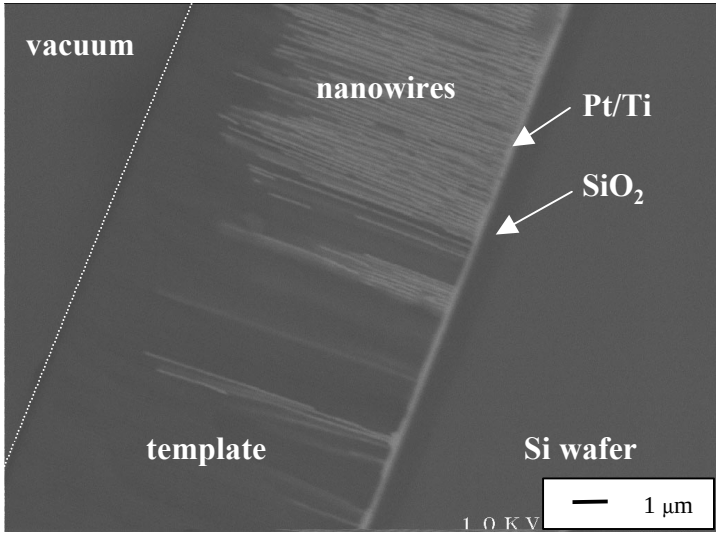

40-nm Bi nanowires deposited in the PAA structure fabricated on a silicon wafer with a conducting adhesion layer.

T-Dependent Resistance and Magnetoresistance of Electrodeposited 200 nm Bi Nanowire Arrays

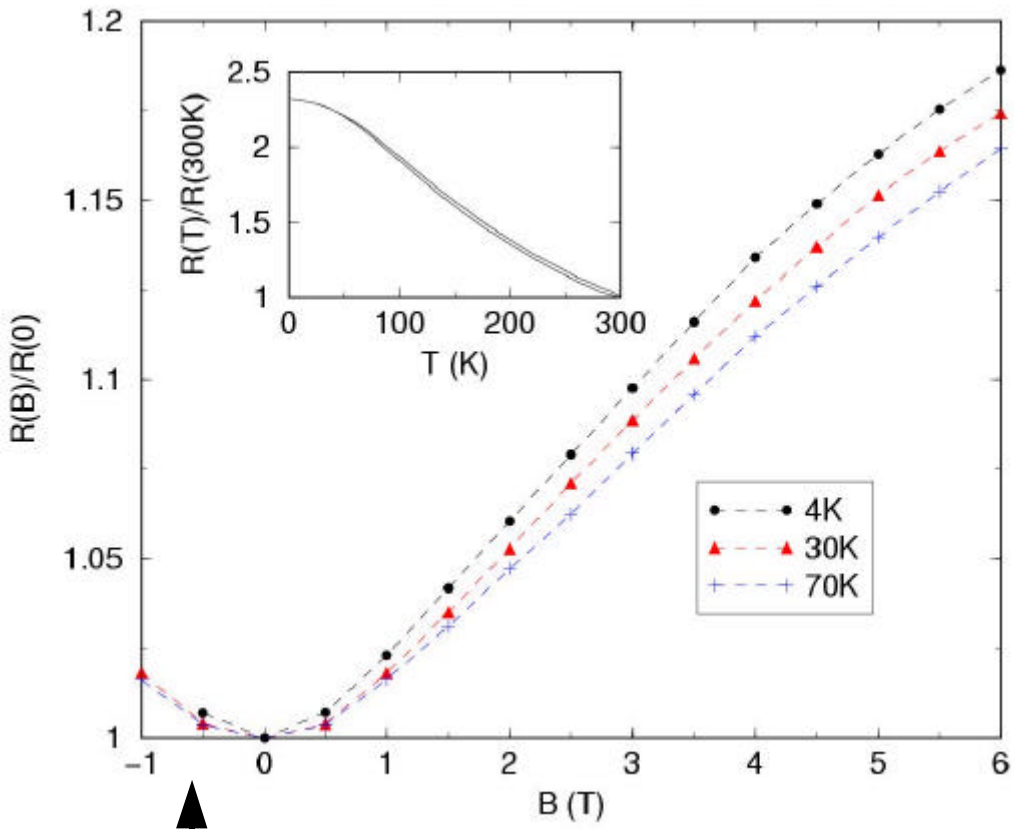

mild electrolyte
(this work)

- The temperature dependence of the electrical properties of our nanowires are identical to those of polycrystalline wires deposited from acidic solutions.
- The magnetoresistance effect is smaller than that observed in single crystal Bi nanowires, due to additional scattering mechanisms in the electrodeposited wires.

acidic electrolyte
(Hong *et.al.*, *JAP* **85**,6184(1999))

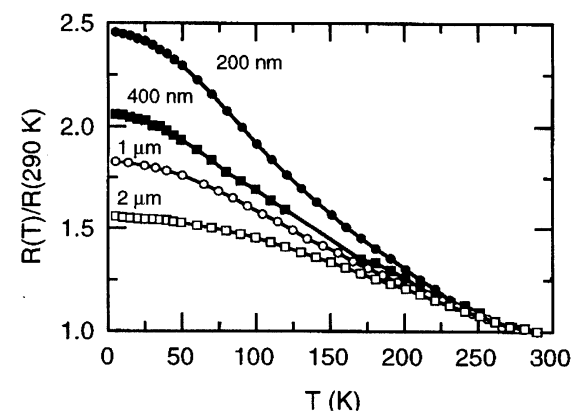

Optical Transmission and Reflection of Bi Nanowires

Measure quantum confinement effects optically:

- Verify band structure and model
- Determine temperature dependence of band parameters
- Possibly measure band gap & free carrier concentration

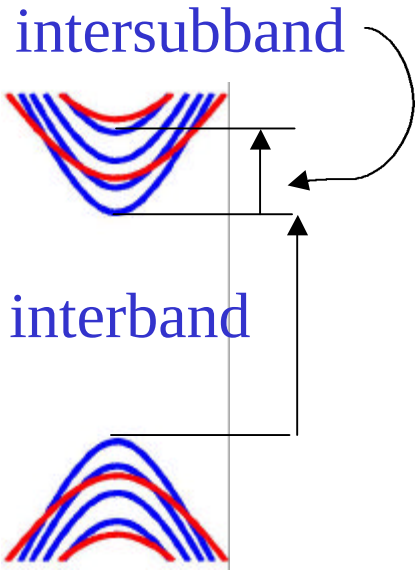

Polarization studies √
FTIR room temperature absorption √
Wire diameter dependence √
Temperature dependence
Electric field dependence

Deducing the Dielectric Function of Bismuth Nanowires

Reflection of Alumina/Bi & Alumina/air

Transmission of Alumina/Bi & Alumina/air

Kramers-Kronig
or
Maxwell's equations

ε_1 of Alumina/Bi & Alumina/air

ε_2 of Alumina/Bi & Alumina/air

$\lambda >> d$

effective medium theory

ε_1 and ε_2 of Alumina

ε_1 and ε_2 of Bi nanowires

sample — template = Bi nanowires

ε_1 and ε_2 Dependence of Bismuth Nanowires on Wire Diameter

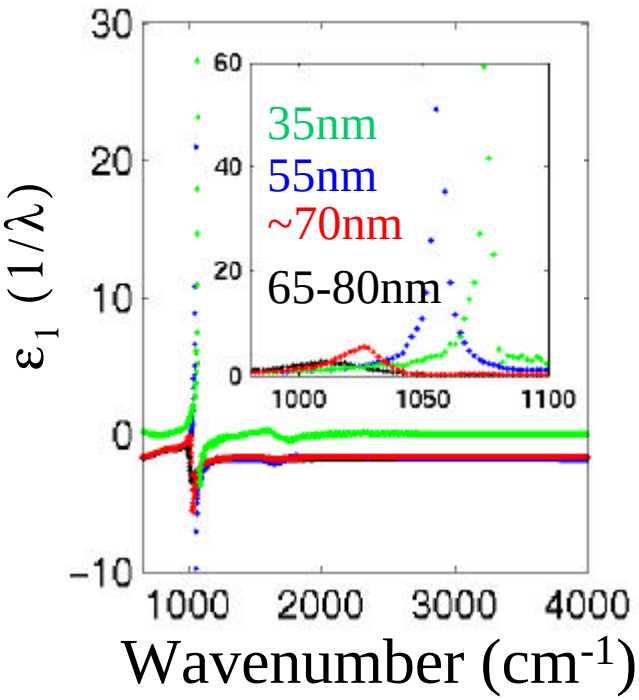

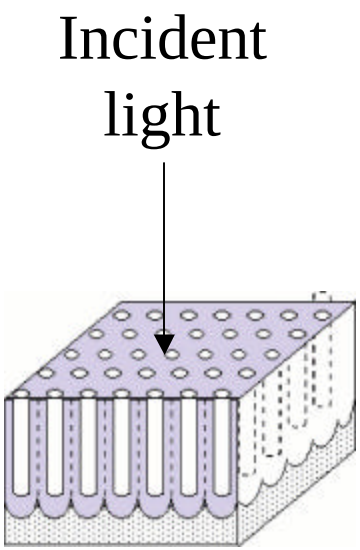

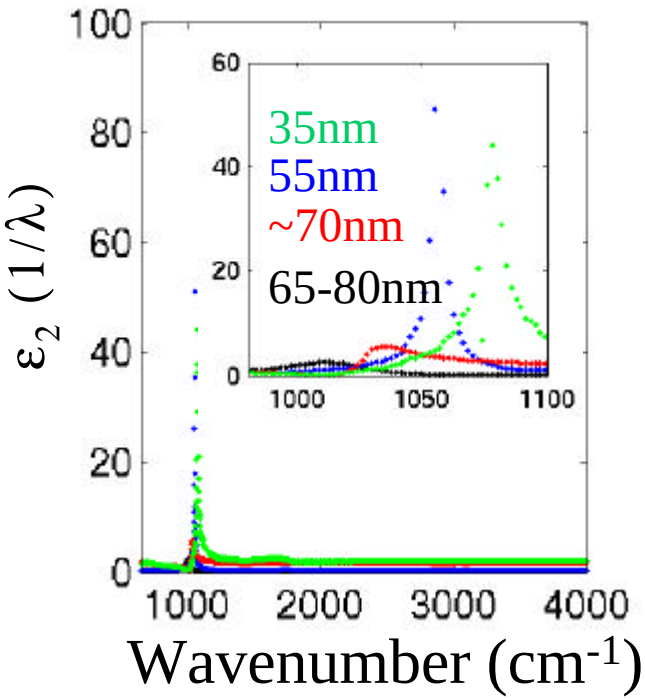

• The dielectric function ($\varepsilon_1 + \varepsilon_2$) of Bi nanowires with different diameters obtained from analysis of reflectivity measurements.

Identifying Optical Absorption Mechanisms

Many absorption mechanisms at similar energy

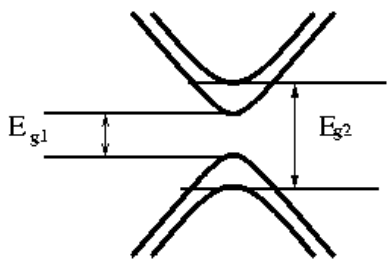

interband

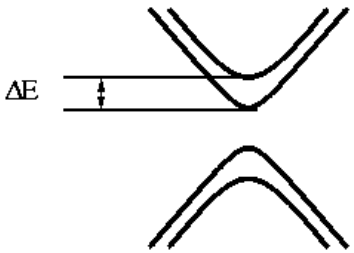

intersubband

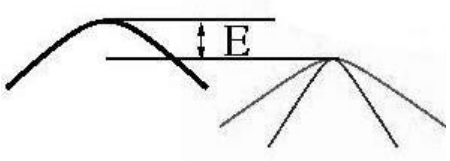

indirect

To separate absorption mechanisms we vary:

diameter

temperature

polarization

Semimetal to Semiconductor Transition

- Transition depends on both wire diameter and temperature
- Different nanowire behaviors in three diameter regimes

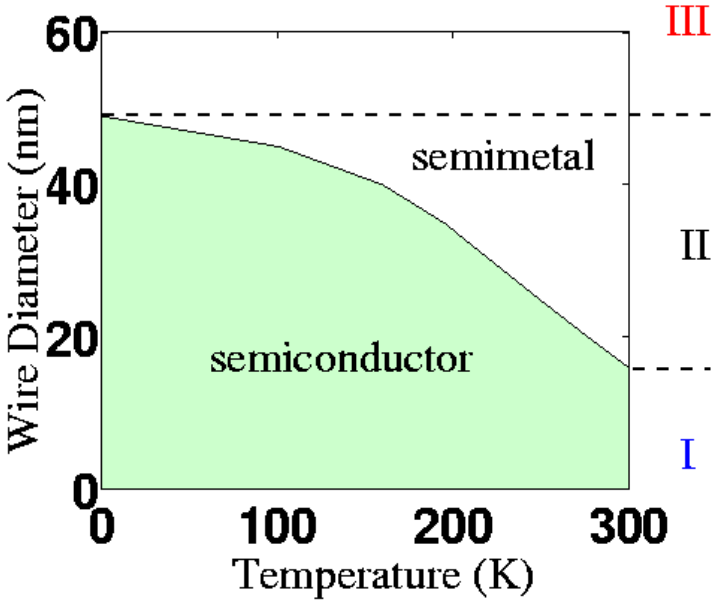

Wire diameter	Anodization Voltage	Bi type
10 nm	20 V	(I) Semiconductor
40 nm	40 V	(II) transition at 160 K
200 nm	160 V	(III) Semimetal

Carrier Pocket Engineering — $Bi_{1-x}Sb_x$ Alloy

- Bi and Sb
  - Group V elements
  - Semimetal in bulk form
  - Completely miscible with each other
  - Introduction of Sb in Bi moves down the *T*-point valence band edge energy relative to the *L*-point edges
  - Provides a promising approach to achieve desirable band structure (i.e., semiconducting) in Bi nanowires

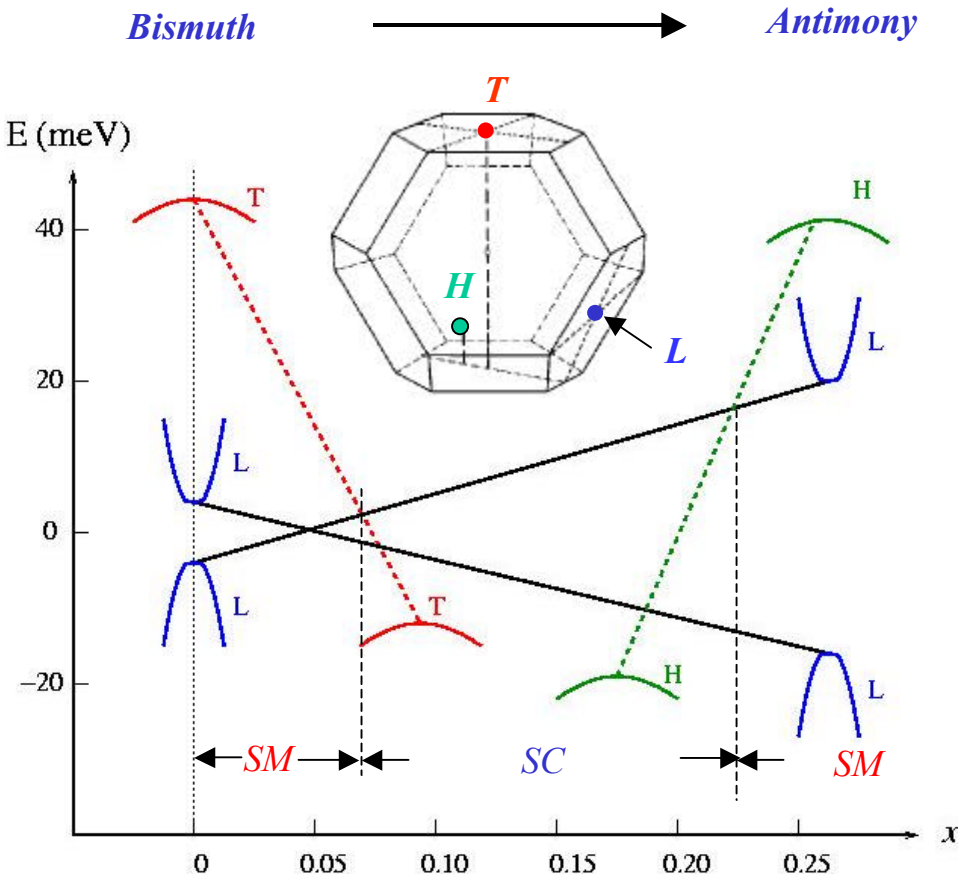

Band structure of $Bi_{1-x}Sb_x$ alloy as a function of Sb concentration x.

SM: Semimetal
SC: Semiconductor

Electronic Band Structures of $Bi_{1-x}Sb_x$ Nanowires

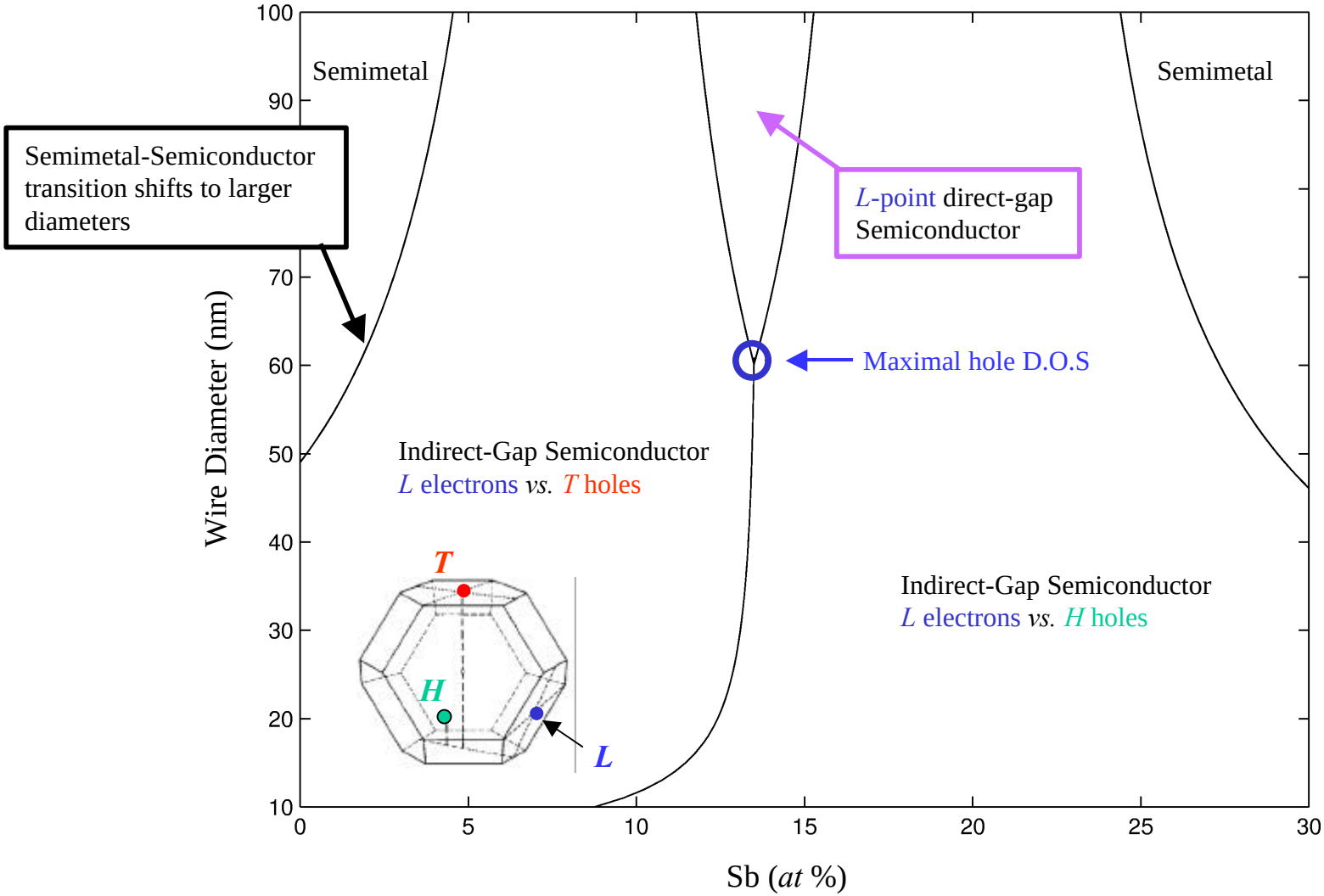

Predicted *ZT* of $Bi_{1-x}Sb_x$ Nanowires

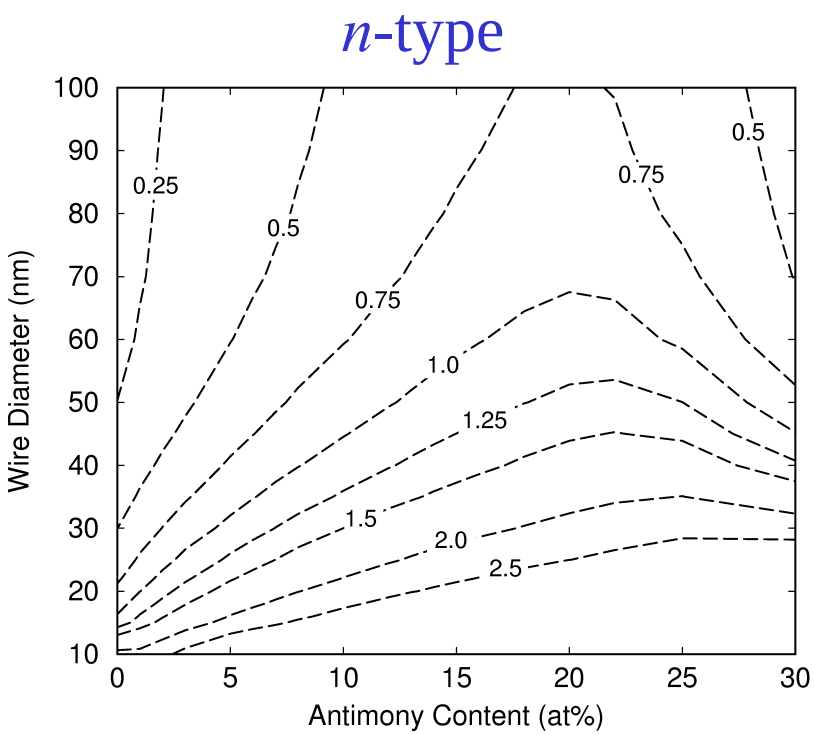

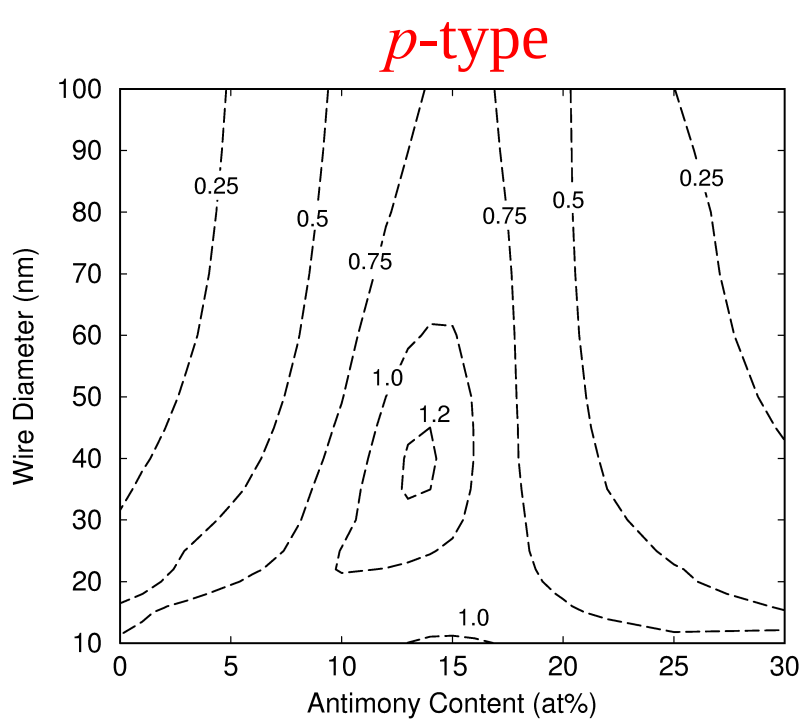

- *ZT* of both *p*-type and *n*-type $Bi_{1-x}Sb_x$ nanowires is increased, and *ZT* performance of practical interest can be achieved at experimentally accessible wire diameters.
- *n*-type and *p*-type nanowires have matched *ZT* (~1.2) at a wire diameter of ~ 40 nm and Sb concentrations of $x \sim 0.13$.

Semimetal-Semiconductor Transition

Prediction

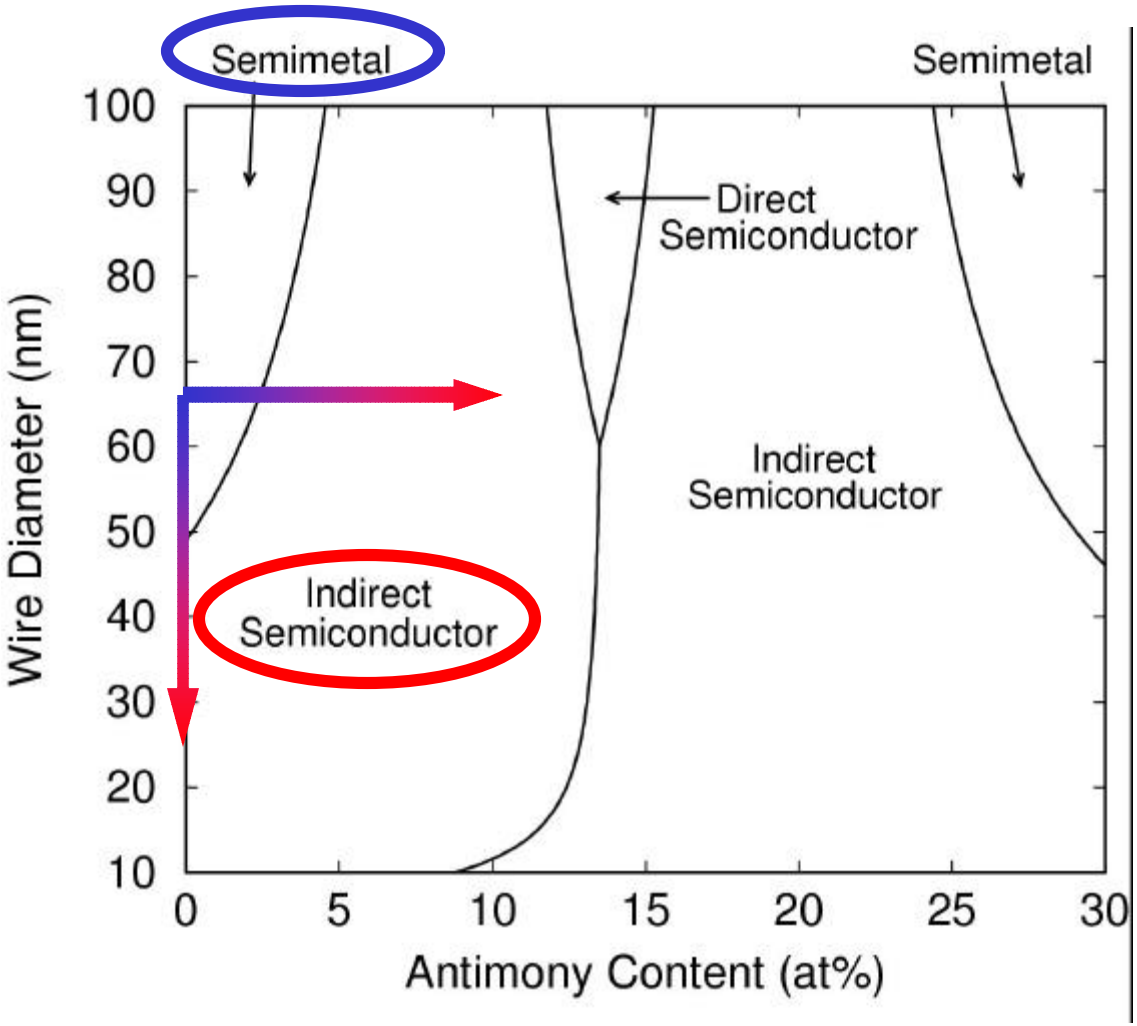

Semimetal-Semiconductor Transition

Observation

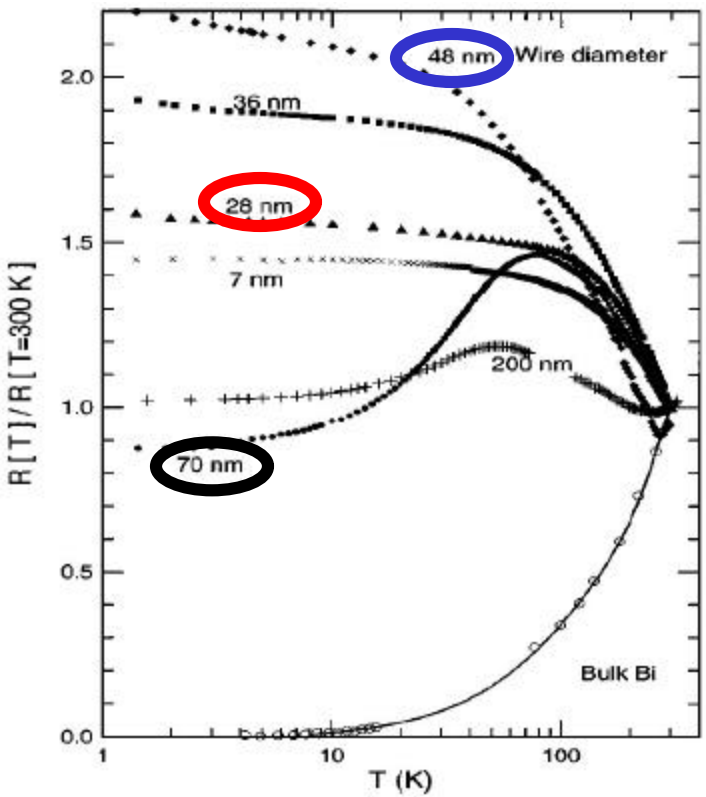

Measured $R(T)$ of pure Bi nanowires.
J. P. Heremans et al.

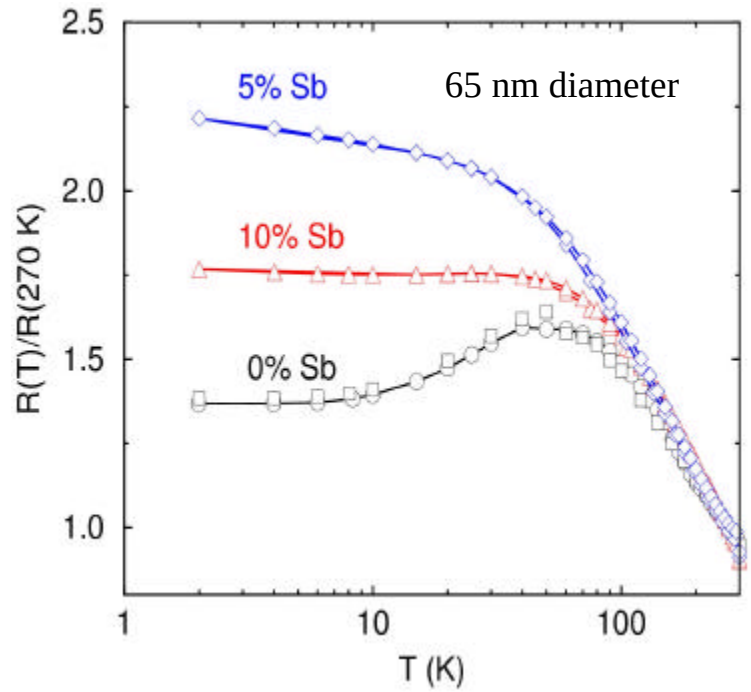

Measured $R(T)$ of 65-nm $Bi_{1-x}Sb_x$ nanowires.

65-nm $Bi_{1-x}Sb_x$ nanowires exhibit semimetal-semiconductor transition behaviors similar to those of pure Bi nanowires.

$R(T)$ of 40-nm Nanowire Arrays

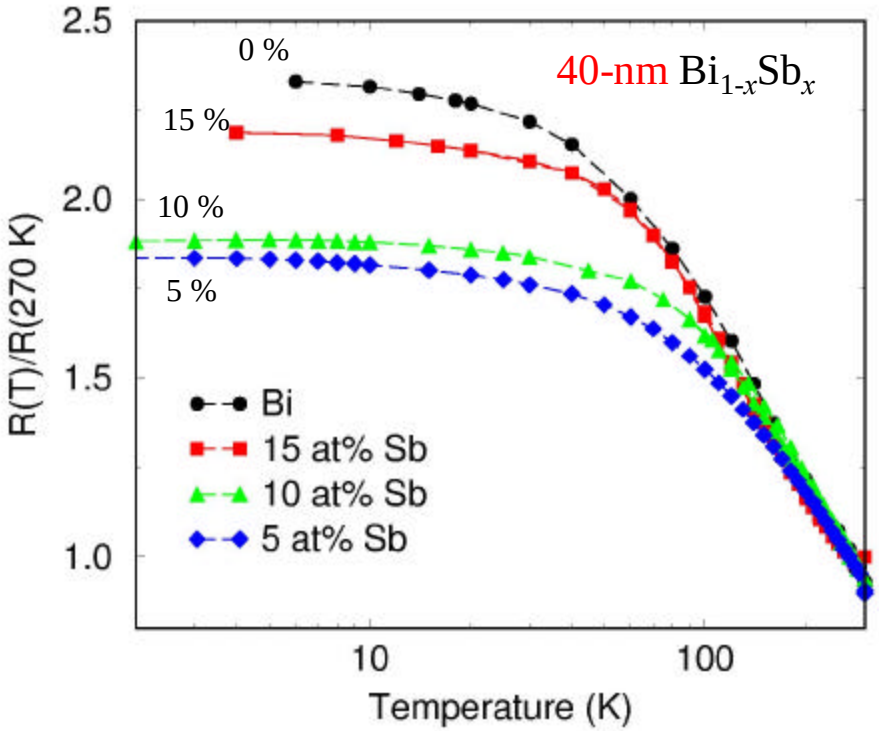

Measured R(T)/R(270 K) of 40-nm $Bi_{1-x}Sb_x$ nanowire arrays with different Sb contents

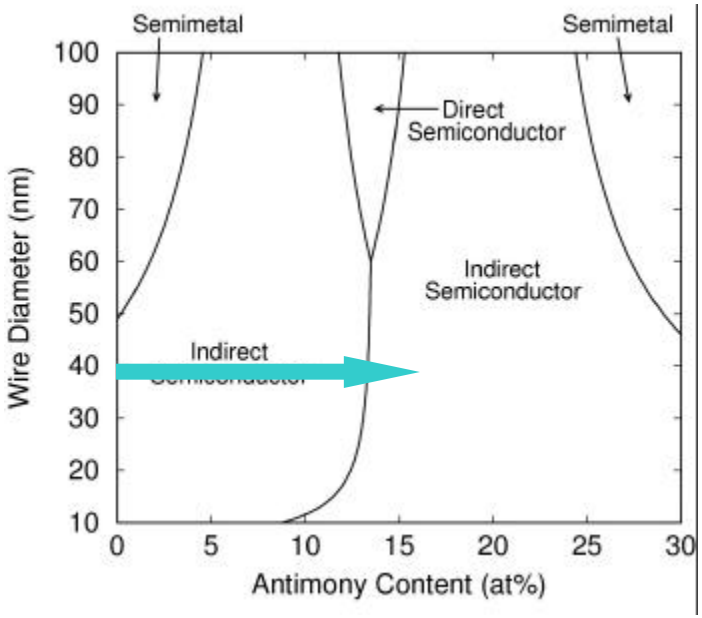

Sb content (x%)	0	5	10	15
R(10K)/R(100K)	1.34	1.19	1.30	1.29

Ratios of the resistance between 10 K and 100 K for 40-nm $Bi_{1-x}Sb_x$ nanowire arrays

Non-monotonic R(T) vs. Sb content

$s = n\sum m_i g_i$ $\quad m_i$: mobility of the each carrier type

$g_i \equiv n_i / n$ $\quad \Delta g = g(10K) - g(100K)$

R(10 K)/R(100 K) ↓ as n(100 K)/n(10 K) ↓
R(10 K)/R(100 K) ↑ as $\Delta\gamma(L)$ ↓
(*L*-point carriers have the highest mobility)

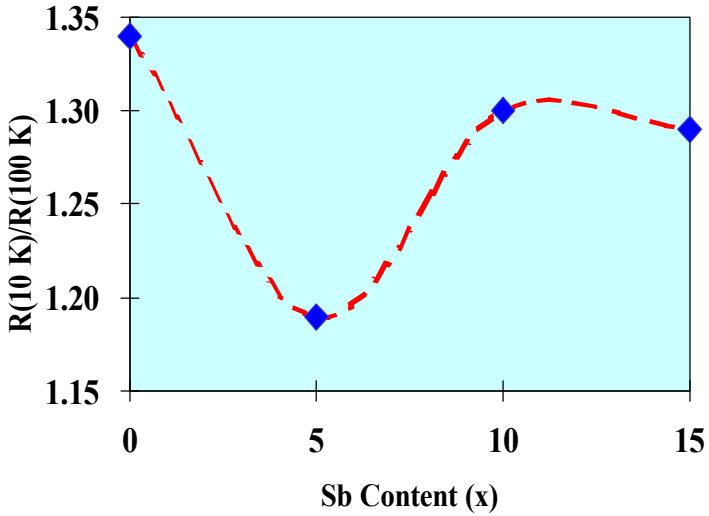

Sb content (x%)	0	5	10	15
R(10K)/R(100K)	1.34	1.19	1.30	1.29

Calculated results:

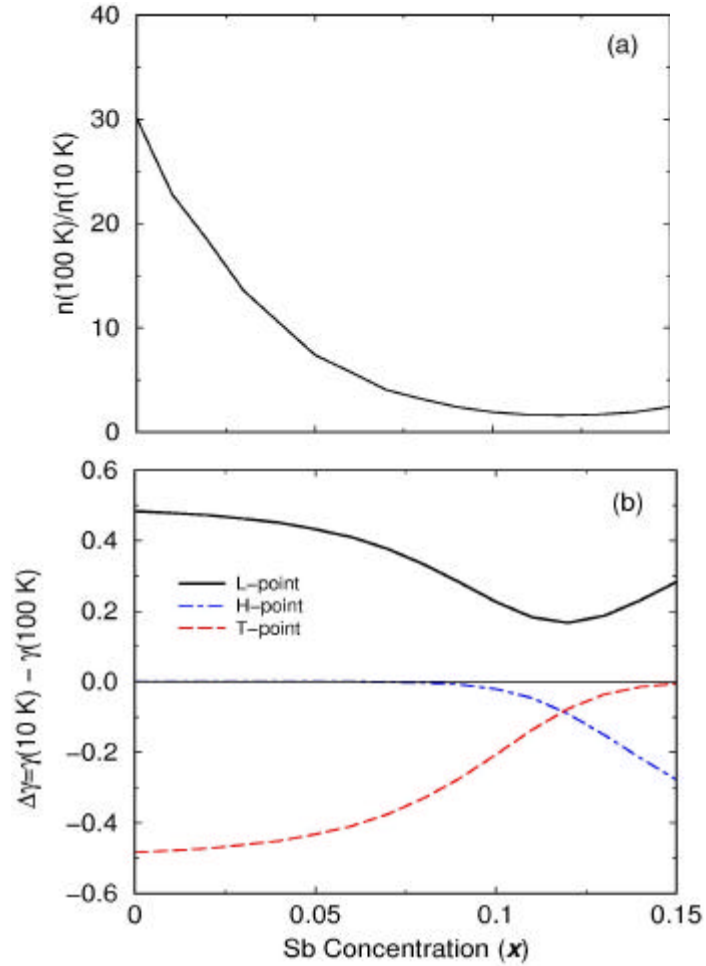

Magnetoresistance:

1D to 3D Transitional Localization

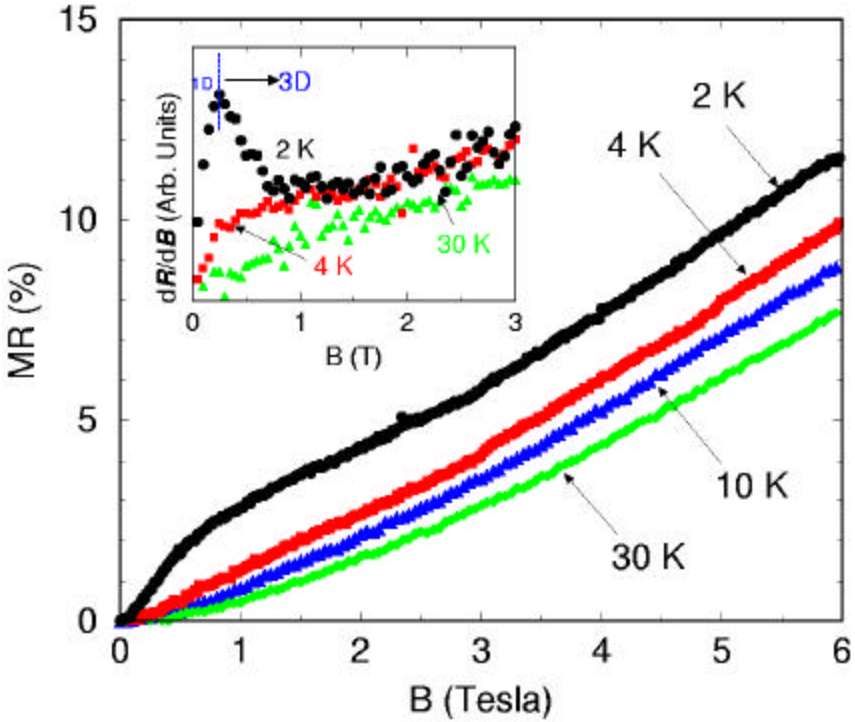

Magnetoresistance of 40-nm $Bi_{1-x}Sb_x$ alloy (x = 0.15) nanowire arrays.
(Inset: first derivative of the *MR* curves with respect to the magnetic field *B*.)

- Magnetoresistance resistance:

$$MR = \frac{R(B) - R(B=0)}{R(B=0)} \approx A_0 B^2$$

- A_0 increases with decreasing T due to decreased phonon scattering
- For $T < 4$ K, the plateau at B ~ 0.75 T indicates a 1D-to-3D transitional localization effect
- Magnetic length:

$$L_H = (\hbar / eB)^{1/2}$$

- 1D to 3D transitional localization:

$$L_H \leq d_W$$

Magnetoresistance II:

Boundary and Impurity Scattering Effect

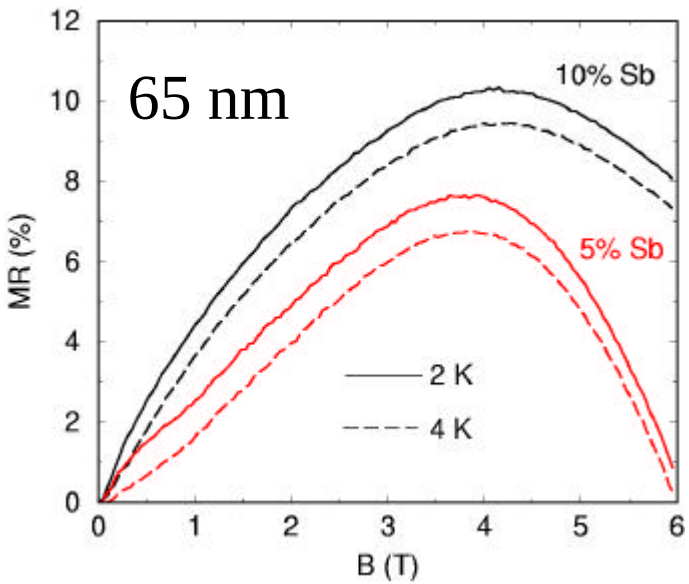

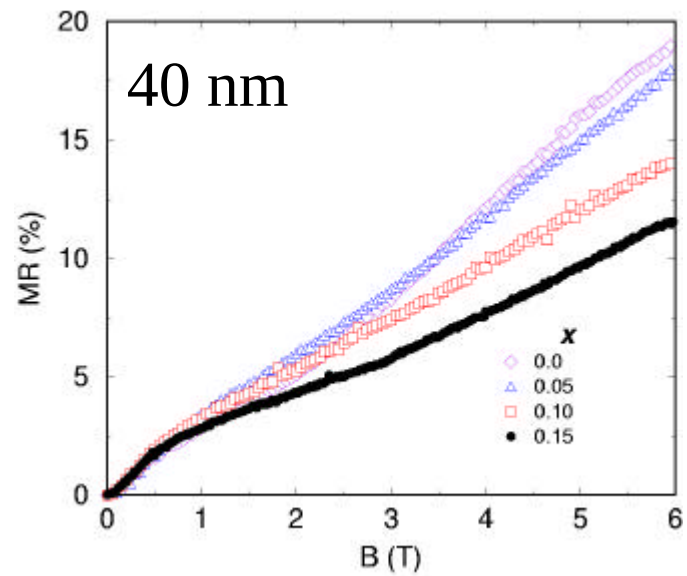

- Magnetoresistance of 65-nm $Bi_{1-x}Sb_x$ nanowire arrays exhibits a maximum at $B \sim 4$ T due to the boundary scattering, suggesting that ballistic transport phenomena may be possible.

- Magnetoresistance of 40-nm $Bi_{1-x}Sb_x$ wires decreases with increasing Sb concentration x, while that of 65-nm wires increases.

Seebeck Coefficient Measurements

(Heater is on top of the thermocouple)

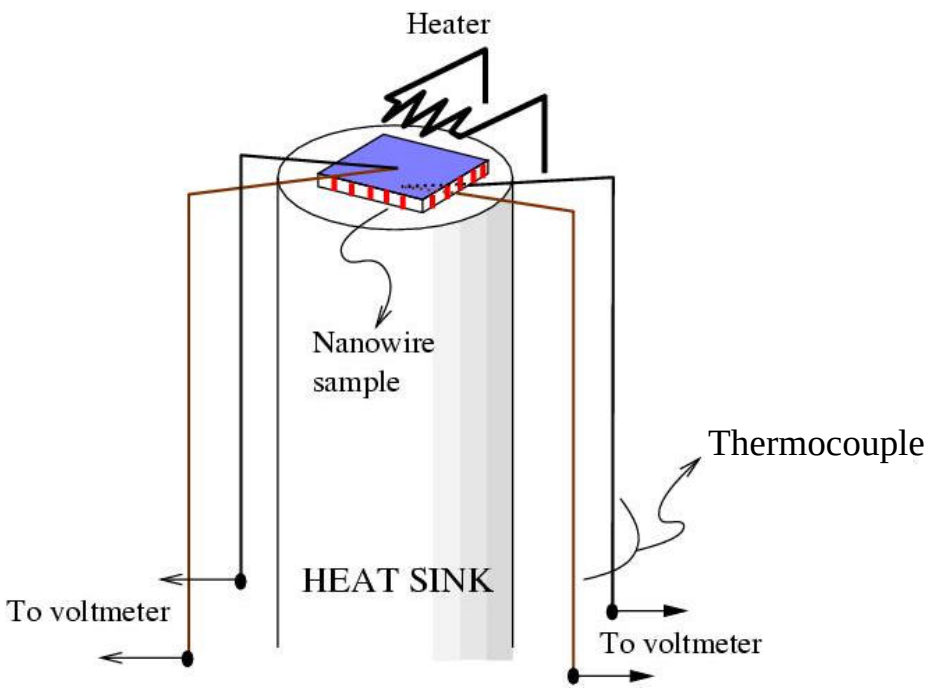

Seebeck Coefficient Measurements

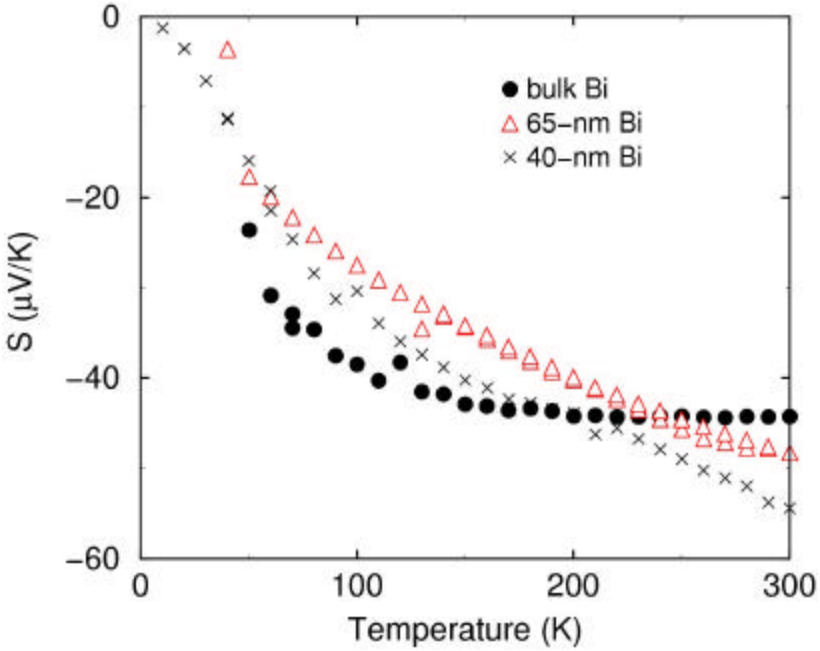

Measured Seebeck coefficient as a function of temperature for 40-nm and 65-nm Bi nanowire arrays

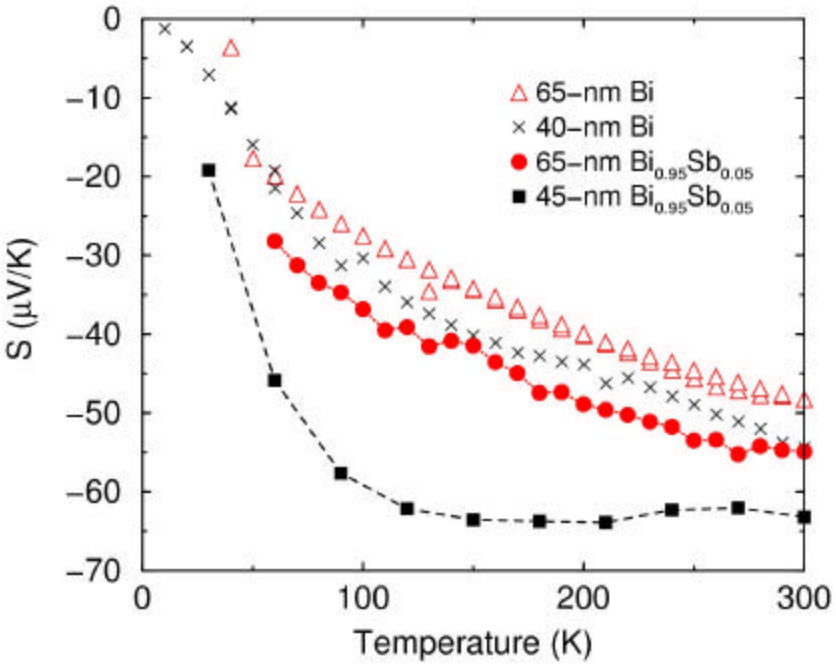

Measured Seebeck coefficient as a function of temperature for 40-nm and 65-nm Bi and $Bi_{0.95}Sb_{0.05}$ nanowire arrays

*Bulk Bi is taken from excess Bi pieces after the pressure injection

New Low-D System:
Segmented Nanowires

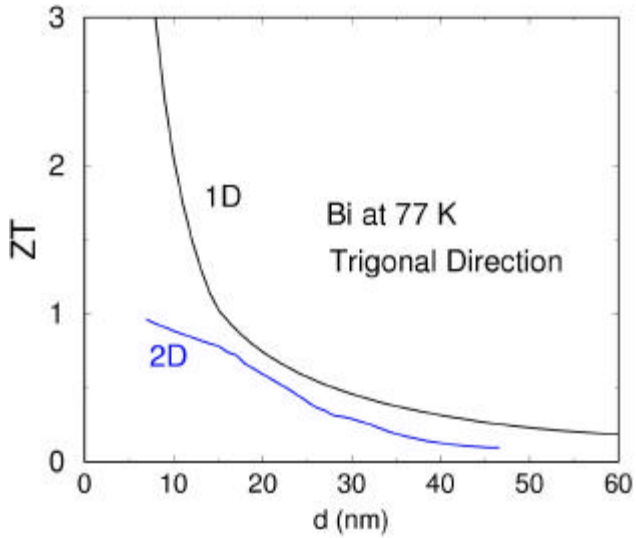

Superlattice (2D)

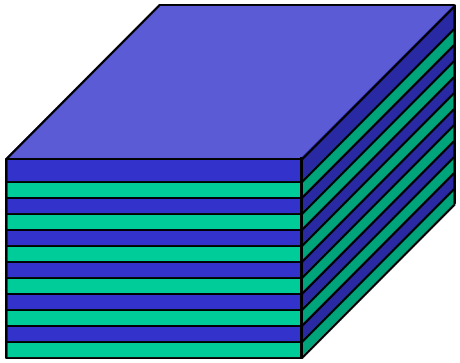

Nanowire (1D)

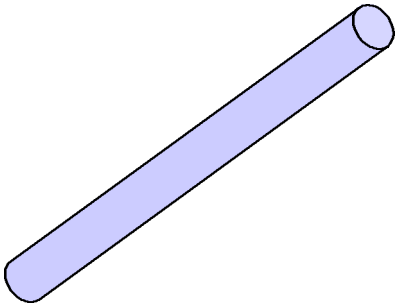

Segmented Nanowire (0D?)

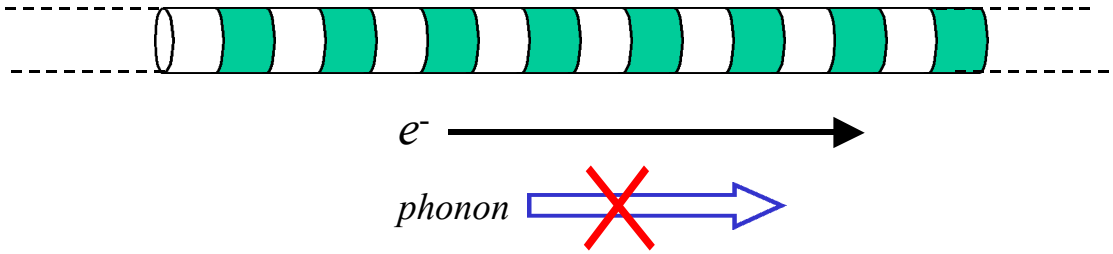

Segmented Nanowire Systems

2D + 1D = Better Thermoelectrics?

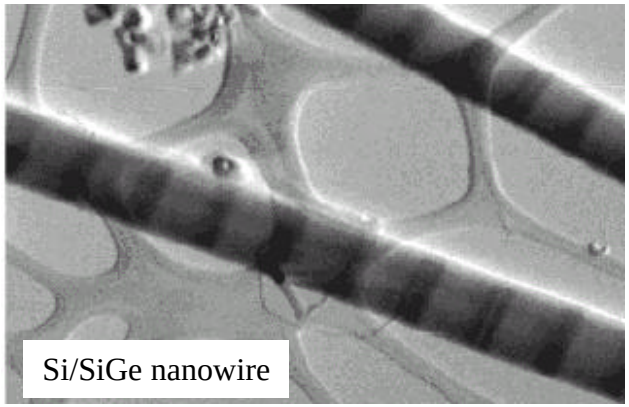

Wu *et al*., Nano Letters (2002)

- Segmented Nanowires:
  - Superlattice in a 1D system
- Motivation
  - To take advantage of both the superlattices and the nanowires to design a better thermoelectric system
  - To substantially reduce the lattice thermal conductivity by increasing the phonon scattering at the segment interfaces
  - To gain insight and understanding of the enhanced thermopower S (and the power factor $S^2\sigma$) in quantum dot arrays *(Harman et al.)* and cross-plane superlattice systems *(Venkatasubramanian et al.)*
- In practice, segmented nanowires can be synthesized using a controlled electrochemical deposition system or laser-ablation approach *(Lieber et al, Samuelson et al., and Yang et al.)*

Calculated $Z_{1D}T$

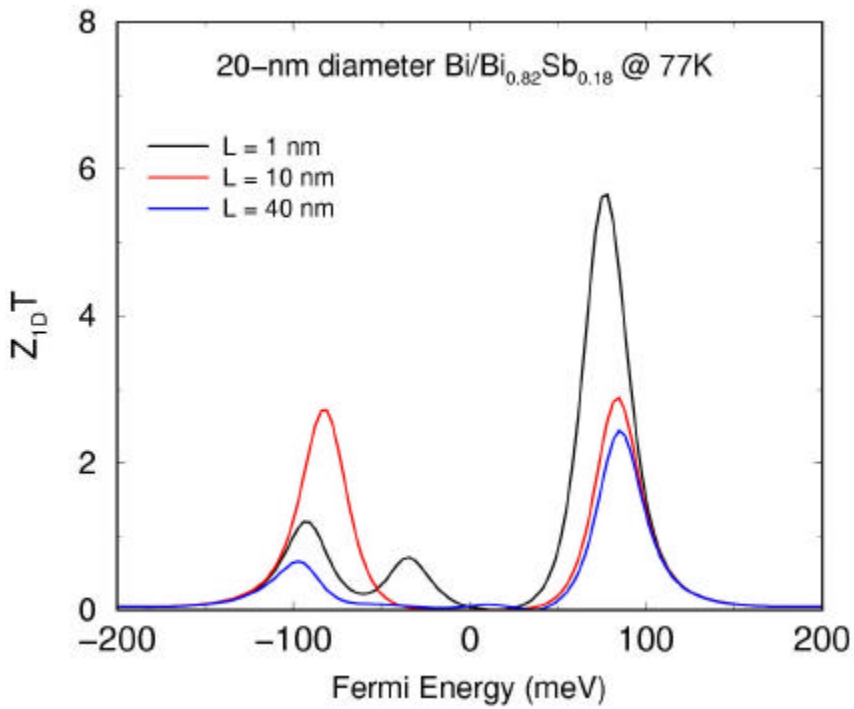

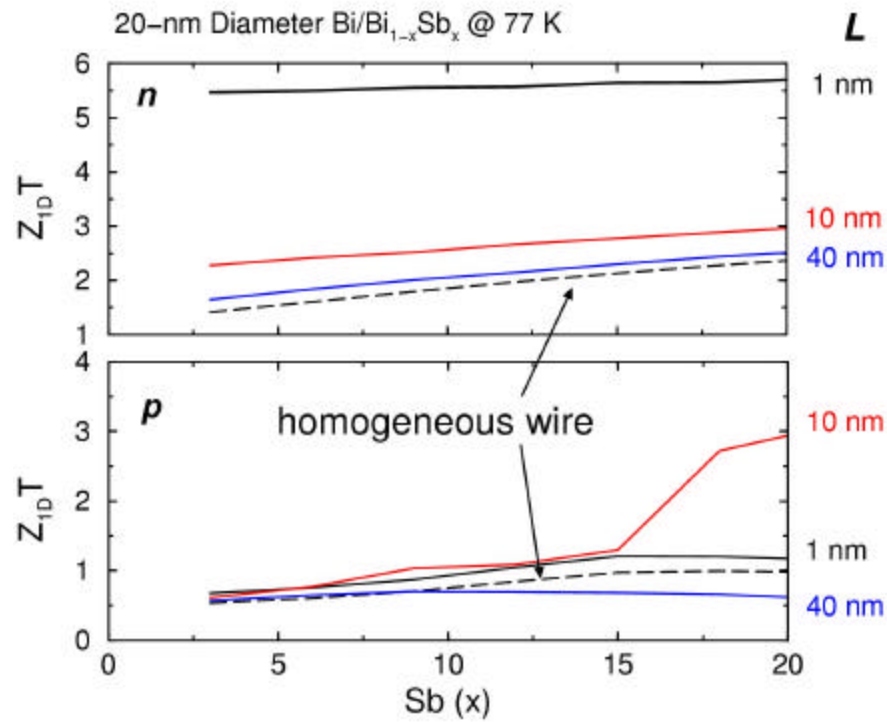

Calculated $Z_{1D}T$ of $Bi/Bi_{0.82}Sb_{0.18}$ segmented nanowires as a function of Fermi energy for different segment lengths L at 77 K.

$Z_{1D}T$ of n and p-type $Bi/Bi_{1-x}Sb_x$ segmented nanowires as a function of Sb content x for different segment lengths L at 77 K.

Major Progress for the Fifth Year (I)

- Improved synthesis of Bi-related nanowires to increase *ZT* and solve practical issues for device performance
  - electrochemical deposition of Bi into alumina template
  - enhancement of mechanical strength and incorporation of electronic circuits by exploiting alumina templates grown on Si substrate
- Applied the carrier pocket engineering concept to $Bi_{1-x}Sb_x$ nanowire systems to further enhance the *ZT* performance. Promising *ZT* values (~1.2) are predicted at experimentally accessible nanowire diameters (~ 40 nm) for both *n*-type and *p*-type wires. This result has both new physics and promise for applications.
- Investigated the electronic transport properties of $Bi_{1-x}Sb_x$ nanowires for various Sb concentrations and wire diameters experimentally and confirmed predictions of model calculations
- Investigated thermoelectric properties of segmented nanowires (e.g., $Bi/Bi_{1-x}Sb_x$ nanowires) for an alternate approach to increase *ZT*
- Improved single nanowire measurement techniques of resistivity and Seebeck coefficient as a function of temperature, diameter, composition

Major Progress for the Fifth Year (II)

- Measured Seebeck coefficient of Bi nanowire arrays to determine the power factor $S^2\sigma$ and to show parameter range where antimony alloying improves performance
- Measured magnetic field-dependent resistance, and results show 1D to 3D localization and boundary scattering effects, indicating a high carrier mobility in the nanowires.
- Measured optical properties of nanowire arrays, for which the wire diameter is much smaller than wavelength of light. Optical absorption results have been related to model calculations.